



12-2000

## An Experimental Study of Low Speed Open Cavity Flows

Abraham J. Meganathan  
*University of Tennessee, Knoxville*

Follow this and additional works at: [https://trace.tennessee.edu/utk\\_gradthes](https://trace.tennessee.edu/utk_gradthes)



Part of the [Mechanical Engineering Commons](#)

---

### Recommended Citation

Meganathan, Abraham J., "An Experimental Study of Low Speed Open Cavity Flows. " Master's Thesis, University of Tennessee, 2000.  
[https://trace.tennessee.edu/utk\\_gradthes/3706](https://trace.tennessee.edu/utk_gradthes/3706)

This Thesis is brought to you for free and open access by the Graduate School at TRACE: Tennessee Research and Creative Exchange. It has been accepted for inclusion in Masters Theses by an authorized administrator of TRACE: Tennessee Research and Creative Exchange. For more information, please contact [trace@utk.edu](mailto:trace@utk.edu).

To the Graduate Council:

I am submitting herewith a thesis written by Abraham J. Meganathan entitled "An Experimental Study of Low Speed Open Cavity Flows." I have examined the final electronic copy of this thesis for form and content and recommend that it be accepted in partial fulfillment of the requirements for the degree of Master of Science, with a major in Mechanical Engineering.

Ahmad D. Vakili, Major Professor

We have read this thesis and recommend its acceptance:

Kenneth Kimble, John E. Caruthers

Accepted for the Council:

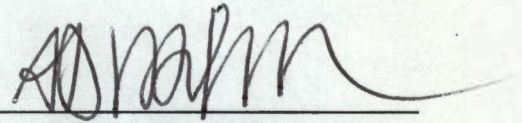
Carolyn R. Hodges

Vice Provost and Dean of the Graduate School

(Original signatures are on file with official student records.)

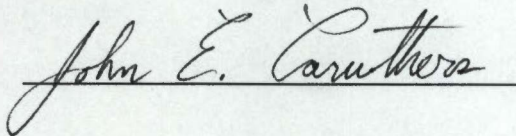
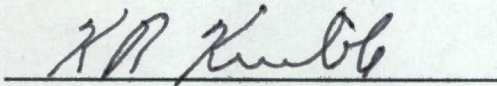
To the Graduate Council:

I am submitting herewith a thesis written by Abraham J Meganathan entitled "An Experimental Study of Low Speed Open Cavity Flows." I have examined the final copy of this thesis for form and content and recommend that it be accepted in partial fulfillment of the requirements for the degree of Master of Science, with a major in Mechanical Engineering'



Ahmad D. Vakili, Major Professor

We have read this thesis  
and recommend its acceptance:



---

Accepted for the council:



Associate Vice Chancellor  
and Dean of The Graduate School

**AN EXPERIMENTAL STUDY OF LOW SPEED OPEN CAVITY FLOWS**

A Thesis  
Presented for the  
Master of Science  
Degree  
The University of Tennessee, Knoxville

Abraham J Meganathan

December 2000

## **ACKNOWLEDGEMENTS**

I gratefully acknowledge the love and support provided by my family in all the endeavors that I have undertaken. I would like to thank my advisor, Dr. Ahmad Vakili for his guidance, encouragement and patience. My thanks and appreciation are also due to Gary Payne, Ricky Meeker, Jim Goodman and other staff of the Gas Dynamics Laboratory. I also thank the other committee members Dr. John Caruthers and Dr. Kenneth Kimble for their suggestions. I would also like to thank fellow graduate students Sekhar Radhakrishnan and Mike Michaud for their help and encouragement throughout the course of this study.

## ABSTRACT

This experimental work is part of an ongoing study aimed at understanding and controlling of cavity instabilities by passive or active steady or unsteady fluid injection. An experimental setup has been designed to quantitatively visualize the flow-field inside the cavity for varying relative dimensions ( $L/D$  ratios of 2.0, 2.67, 3.5 and 4.5,  $W/D$  of 3.33) at low subsonic speeds ranging from 55 ft/sec to 214 ft/sec using Particle Image Velocimetry (PIV).

The results showed that PIV could provide instantaneous velocity and other flow field data inside and above the cavity. The quality of data is good and may be used for validation of numerical predictions. Post-processing of the velocity data provided vorticity and other useful information in the measurement region. Velocity profiles along the shear layer showed shear layer growth towards downstream and a large re-circulation region inside the cavity. As  $L/D$  increased, the re-circulation zone was stronger and was located towards the rear of the cavity. Animations of the vorticity contour images clearly showed vortical disturbances in the shear layer that was convected downstream. It also showed the shear layer oscillating near the trailing edge indicating mass addition and removal process at the trailing edge. Unsteady pressure results showed the selected cavity configurations were oscillating in the selected speed range having peak sound pressure levels ranging from 115 to 133 dB.

## TABLE OF CONTENTS

<u>CHAPTER</u>	<u>PAGE</u>
I INTRODUCTION.....	1
II BACKGROUND AND LITERATURE REVIEW.....	5
Subsonic cavity flow-field types .....	5
Cavity oscillations .....	8
Important parameters.....	18
III EXPERIMENTAL APPROACH.....	20
Wind tunnel.....	20
Cavity Model.....	20
Instrumentation and Data Acquisition.....	23
IV RESULTS AND DISCUSSION.....	31
Pressure measurements.....	31
Velocity measurements.....	39
V CONCLUSIONS AND FUTURE WORK .....	60
LIST OF REFERENCES .....	62
VITA.....	65

## LIST OF FIGURES

<u>Figure</u>	<u>Page</u>
1-1	A basic rectangular cavity configuration.....2
1-2	A schematic representation of cavity oscillation mechanism.....3
2-1	Schematic of different types of cavity flows .....7
2-2	Classification of cavity oscillations from Rockwell and Naudascher [14].....9
2-3	Rossiter’s cavity model.....11
2-4	Pseudo-piston effect from Heller and Bliss [20].....15
2-5	Typical cavity oscillation cycle proposed by Heller and Bliss [20].....16
2-6	Important parameters in cavity flows.....19
3-1	Cavity model installed in UTSI low speed wind tunnel.....21
3-2	Cavity model layout.....22
3-3	Cavity instrumentation layout.....24
3-4	Schematic of the PIV system layout.....27
3-5	Correlation techniques.....30
4-1	Baseline power spectrum for different speeds.....32
4-2	Power spectrum for flow over a cavity of $L/D = 2.0$ .....34
4-3	Power spectrum for flow over a cavity of $L/D = 2.67$ .....35
4-4	Power Spectrum for flow over a cavity of $L/D$ ratio = 3.5.....36
4-5	Power Spectrum for flow over a cavity of $L/D$ ratio = 4.5.....37
4-6	Comparision of Rossiter’s prediction with current data.....38
4-7	Peak Amplitude Vs Speed.....40
4-8	Baseline boundary layer profiles.....43



4-9	Effects of post processing.....	44
4-10	Mean velocity profile and stream trace for $L/D$ ratio = 2.0 at 214 ft/sec.....	45
4-11	Instantaneous velocity contours for flow over a cavity $L/D = 2.0$ and freestream velocity = 214 ft/sec.....	47
4-12	Instantaneous vorticity contours for flow over a cavity $L/D = 2.0$ and freestream velocity = 214 ft/sec.....	48
4-13	Mean velocity profile and stream trace for $L/D$ ratio = 2.67 at 214 ft/sec.....	50
4-14	Instantaneous velocity contours for flow over a cavity $L/D = 2.67$ and freestream velocity = 214 ft/sec.....	51
4-15	Instantaneous vorticity contours for flow over a cavity $L/D = 2.67$ and freestream velocity = 214 ft/sec.....	52
4-16	Mean velocity profile and stream trace for $L/D$ ratio = 3.5 at 214 ft/sec.....	53
4-17	Instantaneous velocity contours for flow over a cavity $L/D = 3.5$ and freestream velocity = 214 ft/sec.....	54
4-18	Instantaneous vorticity contours for flow over a cavity $L/D = 3.5$ and freestream velocity = 214 ft/sec.....	55
4-19	Mean velocity profile and stream trace for $L/D$ ratio = 4.5 at 214 ft/sec.....	57
4-20	Instantaneous velocity contours for flow over a cavity $L/D = 4.5$ and freestream velocity = 214 ft/sec.....	58
4-21	Instantaneous vorticity contours for flow over a cavity $L/D = 4.5$ and freestream velocity = 214 ft/sec.....	59

## NOMENCLATURE

$c$	Speed of acoustic radiation (local speed of sound)
$D$	Depth of the cavity
$f$	Frequency
$f_a', f_b', f_c'$	Primary mode frequencies in the bicoherence spectrum
$k_v$	Vortex to freestream velocity ratio
$L$	Length of the cavity
$m$	Mode of oscillation
$M$	Mach Number
$Re$	Reynolds number ( $UL / \nu$ )
$Pa$	RMS pressure at cavity opening
$Pb$	RMS pressure at base of cavity
$St$	Strouhal number ( $fL / U$ )
$t$	Time
$U$	Velocity
$W$	Width of the cavity
$x$	x-axis
$y$	y-axis
$\alpha$	Acoustic wave emission delay
$\delta$	Boundary layer thickness
$\gamma$	Specific heat ratio
$\lambda$	Wavelength

$\theta$	Momentum thickness
$d\theta/dx$	Shear layer growth rate
$dT, \Delta t$	Time interval between two sequential images
$\Delta x$	Displacement
$\omega$	Vorticity

#### Subscripts

$a$	acoustic
$v$	vortex
$\infty$	freestream
$c$	convective

## *Chapter 1*

### **Introduction**

Cavities in aerodynamic surfaces are known to generate intense steady and unsteady flow disturbances, which can result in large pressure gradients or generate self-sustaining oscillations that radiate acoustic tones from the cavity. These oscillations in turn can cause unsteady loading and vibration of structures, excessive noise and increased drag.

The flow over a rectangular cavity and the geometric variables used in this study are shown in figure 1-1. The boundary layer from upstream of the cavity separates at or near the leading edge forming a free shear layer and traverses the length of the cavity before periodically reattaching at the trailing edge. The mechanism (shown in figure 1-2) producing cavity oscillations consists of the creation of free shear layer perturbations, amplification and downstream convection of the perturbations, interaction of the perturbations with the trailing edge and production of upstream influences[1]. The perturbation may manifest itself as an oscillation of the free shear layer, a vortex or other vortical fluctuations. The upstream influences are generally pressure disturbances and travel through the cavity, the free shear layer or the freestream when the flow is subsonic.

Suppression of cavity oscillations has been attempted with different levels of success by modifying different parts of the cavity flow. Techniques for suppression of cavity oscillation include direct and indirect free shear layer alteration (venting[2] and mass injection[3] from

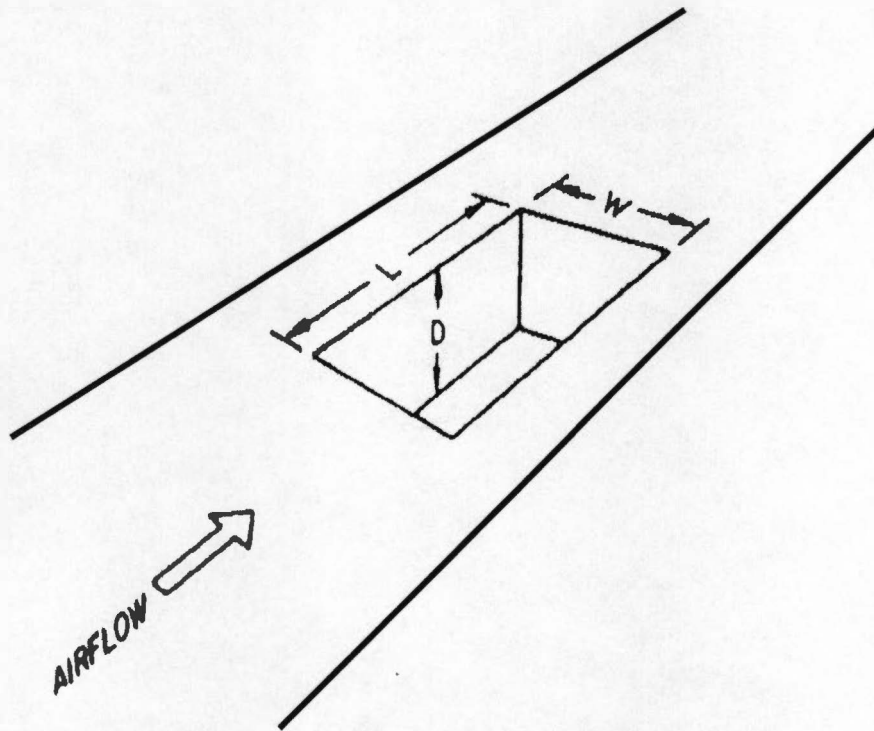


Figure 1 – 1. A basic rectangular cavity configuration, definition of characteristic dimensions

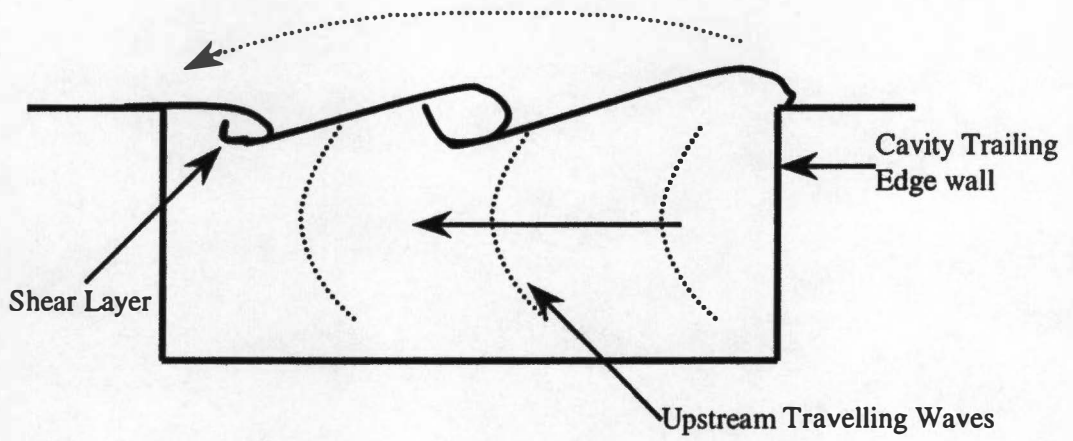


Figure 1 – 2. A schematic representation of cavity oscillation mechanism

the cavity floor), separation and reattachment alteration (ramps[4]) and upstream boundary layer alteration (spoilers [5], vortex generators[6] and upstream mass injection[8,9]). Most of the recent experimental studies are focused on high speed flows, primarily transonic and supersonic flows, and the suppression of cavity oscillations. The works of Vakili et al.[7,8] established the potential for successful suppression of cavity oscillations by passive or active steady or unsteady fluid injection upstream of the cavity.

Though extensive efforts have been made on the characterization and control of cavity flows, lack of detailed quantitative measurements inside the cavity makes it difficult to understand (a) the non-linear development of turbulent cavity shear layer, and (b) interaction of the disturbances (acoustic or other) with the shear layer to excite the flow instabilities. This knowledge is very important to achieve efficient control of flow over cavities.

With this as the broad objective of the ongoing study, this thesis will focus on (a) making detailed measurements over and inside of open cavities using Particle Image Velocimetry (PIV) and pressure measurements inside selected cavities at low speeds, and (b) identifying instantaneous flow structures that are part of the overall behavior of the flow. It is anticipated that the results of this study would shed more light on understanding the physical process in cavity flows. It is also anticipated that this study would be used for validation of numerical prediction of cavity flows at low speeds.

## Background and Literature Survey

### 2.1 Subsonic cavity flow-field types

Flow over cavities can be classified based on

(i) Length to depth ratio

(a) Shallow cavities

These cavities have their longest dimension in the streamwise direction ( $L/D > 1$ ). Shallow cavities tend to resonate primarily in lengthwise mode.

(b) Deep cavities

These cavities have their longest dimension perpendicular to the streamwise direction ( $L/D < 1$ ). Deep cavities tend to resonate primarily in depth mode.

(ii) Shear Layer reattachment

(a) Closed flow

In closed cavities, the flow separates at the leading edge of the cavity and reattaches at some point along the cavity floor and separates again before reaching the trailing edge. Typically it has been observed to occur for an  $L/D$  ratio greater than or equal to 13[10]. The drag of closed cavities is substantially higher than that of open cavities[11]



(b) Open flow

In open cavities, the flow spans the length of the cavity and a shear layer is formed over the cavity. It occurs in cavities with  $L/D$  ratios less than or equal to 10. In this type of flow, cavity resonance can be sustained which generates high intensity acoustic tones[12].

(c) Transitional flow

The flow turning into the cavity may or may not impinge on the cavity floor before turning out and exiting. This occurs in cavities with  $L/D$  ratios between 10 and 13. Figure 2-1 shows these flow types.

(iii) Cavity Oscillation

(a) Fluid Dynamic Oscillation

These are cavity oscillations that are driven solely by the inherent instability of the shear layer. Selective amplification of the instabilities and the pressure disturbances at the trailing edge are necessary. They are limited to situations where the cavity length is less than one-fourth of the acoustical wavelength. The length is too short for a standing wave to be present inside the cavity[13].

(b) Fluid Resonant Oscillation

These are cavity oscillations that result from a coupling of the inherent instability of the shear layer with one or more of the acoustic resonant modes of the cavity and are characterized by strong acoustic resonances inside the cavity. They occur when the shedding frequencies are sufficiently high and the acoustic wavelengths sufficiently short as to allow

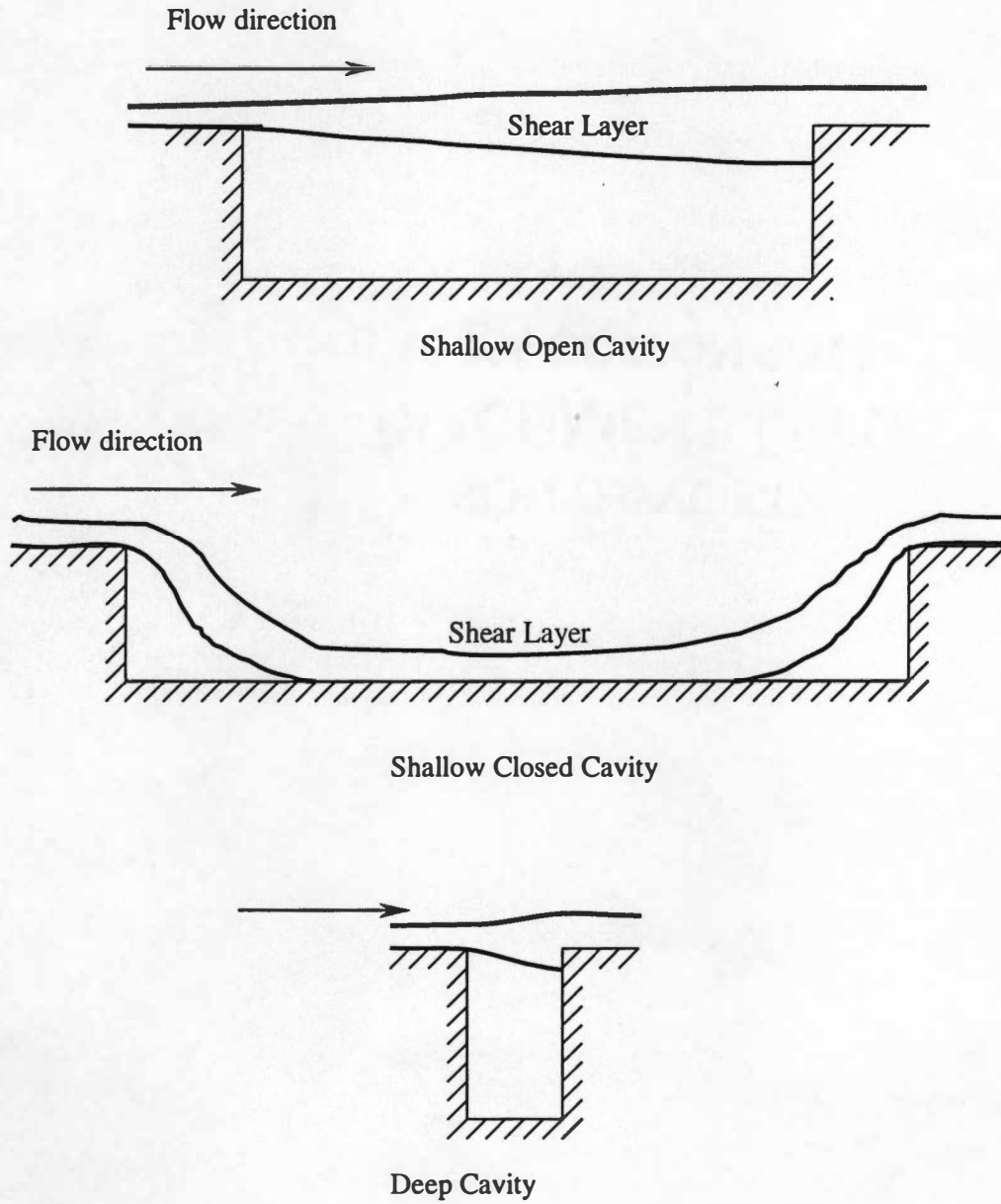


Figure 2 – 1. Schematic of different types of cavity flows

for standing waves inside the cavity. The acoustic resonances provide the upstream travelling influence.

(c) Fluid Elastic Oscillation

Fluid elastic oscillations result from the coupling of inherent instability of the shear layer with elastic movement of part or all of the cavity-bounding walls. The movement of the structure provides the pressure and acoustic resonance effects. Structural properties are important in these oscillations.

The classification of cavity oscillations as proposed by Rockwell and Naudascher[14] is shown in figure 2-2. In actual situations, these oscillations may occur simultaneously.

## 2.2 Cavity Oscillations

Cavity oscillations are rapid fluctuations of the pressure, density and velocity of the fluid inside a cavity which has been exposed to flow above the cavity. Studies of the phenomenon of cavity oscillations covering a wide range of geometrical and flow parameters were performed by Karamcheti[15]. He studied the acoustic field of two-dimensional shallow cavities in the Mach number range of 0.25 to 1.5 using Schlieren and Interferometric observations. He noticed that for a fixed freestream Mach number and depth, there exists a minimum length below which there was no sound emission and that the minimum length was inversely proportional to the Mach number. In a non-oscillating cavity, the shear layer bridges the cavity without strong interaction with the trailing edge. He also observed that the radiation was more intense for a laminar upstream boundary layer than for a turbulent upstream boundary layer.



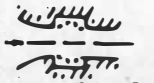


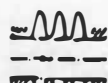

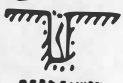










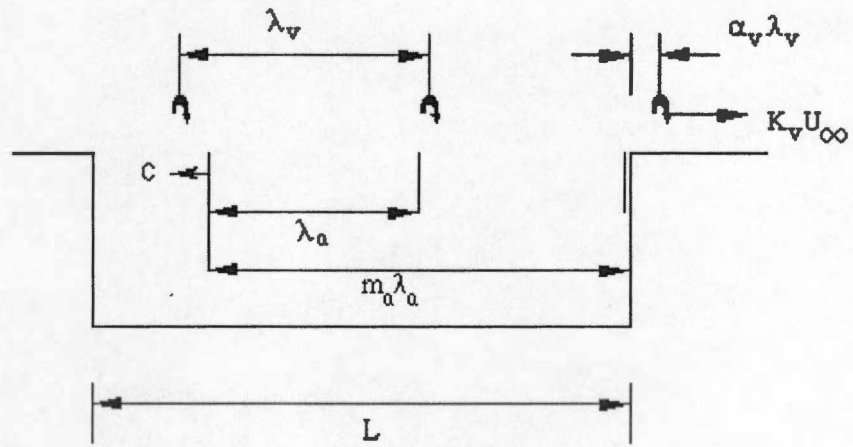
Type	Basic Cavity	Variations of Basic Cavity			
<b>Fluid-Dynamic Shear Layer Instability</b>	 SIMPLE CAVITY	 AXISYMMETRIC EXTERNAL CAVITY   AXISYMMETRIC INTERNAL CAVITY	 CAVITY-PERFORATED PLATE   GATE WITH EXTENDED LIP	 BELLOWS	
<b>Fluid-Resonant Shear Layer Instability and Cavity Acoustic Resonances</b>	 SHALLOW CAVITY   DEEP CAVITY	 SLOTTED FLUME   WALL JET WITH PORT	 CAVITY WITH EXTENSION   BRANCHED PIPE	 HELMHOLTZ RESONATOR   CIRCULAR CAVITY	
<b>Fluid-Elastic Shear Layer Instability and Cavity Elastic Deformation</b>	 CAVITY WITH VIBRATING COMPONENT	 VIBRATING GATE	 VIBRATING BELLOWS	 VIBRATING FLAP	

Figure 2 – 2. Classification of Cavity Oscillations (reproduced from Rockwell and Naudascher[14])

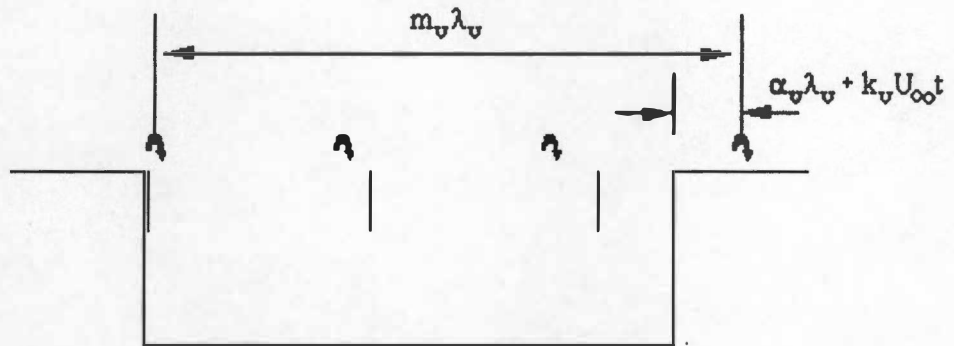
Roshko[16] studied the pressure and velocity flow fields in cavities of  $L/D$  ratios ranging from 10.6 to 62.5 at low speeds (75 ft/sec to 210 ft/sec). He observed that the cavity flow was open for  $L/D$  ratios less than or equal to ten. He suggested that the shear layer impact on the trailing edge might be important in the sound production in cavities. He concluded that the drag increment due to cavity is almost entirely accounted for by the pressures on the walls.

Plumlee et al.[17] proposed that the observed discrete tones were the result of cavity resonance. They suggested that the frequencies of the tones were identical to those which corresponded to the maximum acoustic response of the cavity. According to this theory, the entire turbulent shear layer which spans the open end of the cavity provides a broad band noise source which drives the cavity oscillation. The response of the rectangular cavity to this broad band excitation is instrumental in selecting certain narrow band frequencies for amplification. But when experiments showed that flows with laminar upstream boundary layer produced louder tones, this line of reasoning was contradicted.

Rossiter[5] examined a series of rectangular cavities at low and transonic Mach numbers (0.4 – 1.2). He concluded that both periodic and random components of unsteady pressures could be present in the cavities. In general, the random component predominates in shallow cavities of  $L/D > 4$  and the periodic component predominates in cavities having  $L/D < 4$ . The random component is more intense near the rear wall of the cavity. His high-speed shadowgraph motion pictures showed the periodic emission, downstream convection and amplification of the shed vortices. He also indicated that periodic components are due to an acoustic resonance in the cavity. Based on these observations he proposed a simple model (figure 2-3) consisting



(a) Time = 0 Sound wave leaves rear lip



(b) Time =  $t$  Vortex leaves front lip

Figure 2 – 3. Rossiter's cavity model

of periodic vortex emission, which is convected downstream and impinges on the trailing edge. After a small time delay, an acoustic wave is emitted from the trailing edge which travels upstream and perturbs the shear layer at the leading edge. He derived an empirical formula to predict the excitation frequency given by

$$St = \frac{fL}{U_\infty} = \frac{m - \alpha}{M + \frac{1}{K_v}}$$

where,

St = Strouhal number

f = Frequency

L = Length of the cavity

$U_\infty$  = freestream velocity

M = Mach number

$K_v = U_s/U_\infty$  is the ratio of the shear layer velocity to free stream velocity

m = mode number

$\alpha$  = empirical constant that accounts for the phase differences between (a) upstream arrival of the acoustic wave and subsequent vortex shedding (b) downstream interaction with the leading edge and subsequent acoustic radiation

This model agreed well with experimental data in the range of 0.4 to 1.5. Rossiter's assumption that the sonic speed inside the cavity is the same as the freestream sonic speed under-predicted the Strouhal number for Mach numbers above 1.5.

Heller, Holmes and Covert[18] modified the formula by assuming that the freestream stagnation sonic speed equals the cavity sonic speed. The modified Rossiter equation is

$$\frac{fL}{U_{\infty}} = \frac{m - \alpha}{\left[ \frac{M_{\infty}}{\left[ 1 + \frac{\gamma - 1}{2} M_{\infty}^2 \right]^{\frac{1}{2}}} + \frac{1}{K_v} \right]}$$

where ,

$\gamma$  = ratio of specific heats.

These formulas do not predict whether a self-sustained oscillation will occur. Neither can they predict the amplitude of the oscillations. The models do not describe how the acoustic wave interacts with the shear layer at the leading edge or how the acoustic disturbance is generated at the trailing edge wall in the first place.

Bilanin and Covert[19] improved on Rossiter's feedback model by relating the driving mechanism of oscillations to the instabilities of the free shear layer. The shear layer at the mouth of the cavity is prone to Kelvin-Helmholtz instabilities. They assumed that the shear layer is being agitated periodically at the upstream lip of the cavity. This excites the flow instability waves of the shear layer as they propagate upstream. This fluctuating motion of the shear layer at the trailing edge of the cavity induces a periodic inflow of external flow into the cavity and half a period later a discharge of cavity fluid into the external flow. Bilanin and Covert attributed this mass inflow and outflow as the source of acoustic radiation. The acoustic disturbances then propagate upstream inside the cavity without disturbing the shear layer and excite the shear layer at the leading edge. Using a thin vortex sheet and a noise



source at the downstream corner of the cavity, they modeled the flow and predicted the excitation frequencies which agreed well in high supersonic Mach number flows.

Heller and Bliss[20] using watertable visualization, observed periodic addition and removal of mass at the trailing edge in shallow cavities. They called this the “pseudo-piston” effect (shown in figure 2-4), which generates forward travelling waves in the cavity that reflect from the front bulkhead and become rearward travelling waves. They also identified that the unsteady shear layer motion is responsible for the trailing edge mass addition and removal. The typical oscillation cycle is shown in figure 2-5.

Sarohia[21] examined ring cavities with dimensions of 0.05” to 0.875” in depth and 0” to 2” in length at speeds between 0 ft/sec and 80 ft/sec. Sarohia found a non-dimensional minimum length (ratio of length to momentum thickness) for oscillations to occur in laminar flows. He concluded that the phenomenon of oscillations in low-speed flows over cavities is not an acoustic resonance phenomenon in the longitudinal direction. These oscillations result from propagating disturbances that get amplified along the cavity shear layer. He also observed that the presence of strong cavity oscillations contributed to a large growth of the shear layer.

Tam and Block[22] investigated cavities in the low subsonic range ( $M < 0.4$ ) and suggested that normal mode resonance dominated at Mach numbers less than 0.2 even for shallow cavities. Their model accounted for acoustic emission at the trailing edge as well as from the front, back and bottom of the cavity. They modeled the shear layer as an infinitesimally thin sheet and the acoustic disturbance at the trailing edge as a simple acoustic point source. Later they corrected it for the finite shear layer thickness based on a mean momentum thickness.

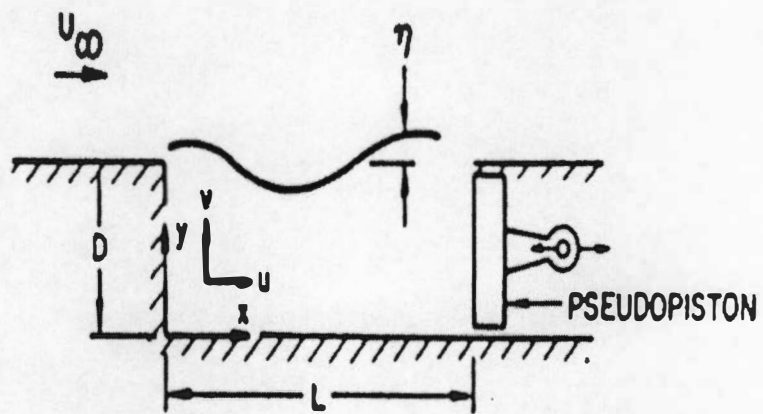


Figure 2 – 4. “Pseudo-piston” Effect ( reproduced from Heller and Bliss [20])

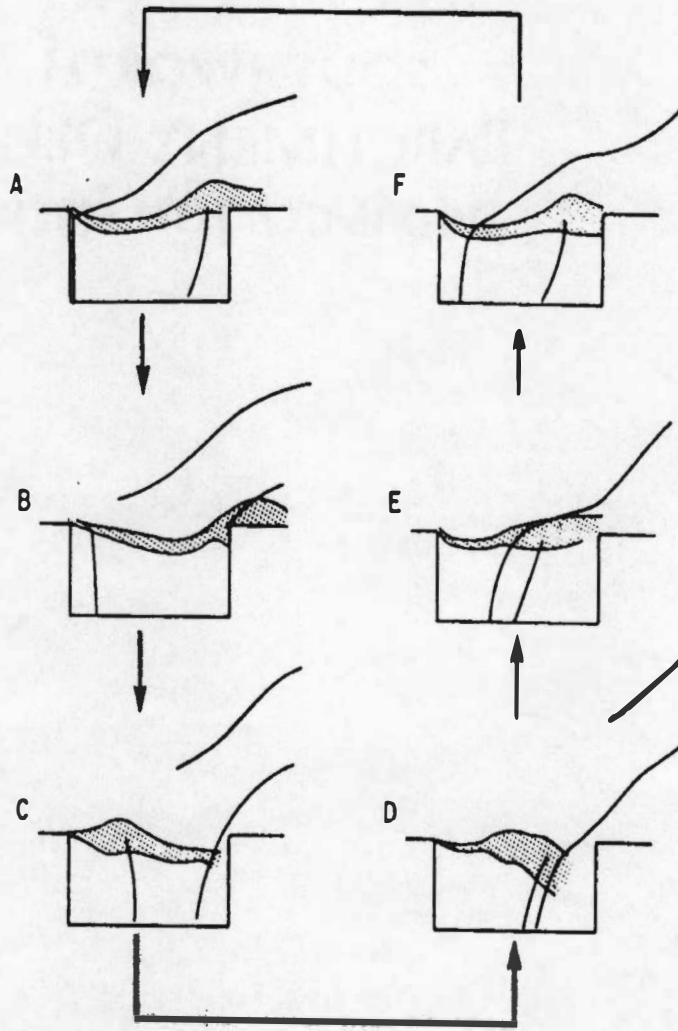


Figure 2 – 5. Typical cavity flow oscillation cycle as proposed by Heller and Bliss [20]

Based on this model, they suggested that the ratio of the cavity length and momentum thickness of the shear layer was important.

Catafesta et al.[23] studied the cause of additional peaks in the spectrum, particularly at low frequencies and the presence of multiple peaks in the power spectrum. They used time-frequency methods namely the Short Time Fourier Transform (STFT) and the continuous Morlet wavelet transform. They proposed a hypothesis that when three Rossiter modes ( $f_c > f_b > f_a$ ) are present and satisfy the relation  $(f_c - (f_a + f_b)) = \Delta f \approx 0$ , significant nonlinear coupling can occur between the modes leading to a low frequency amplitude modulation of the primary modes at  $f_m = \Delta f$  and larger than normal SPL. Even when this condition is not satisfied, the different interactions between the primary nodes create a low frequency mode that appears in the power spectrum and amplitude modulates the Rossiter modes.

Eric et al.[24] conducted detailed measurements of the cavity shear layer, the internal regions of the cavity and the acoustic near field with an optical deflectometer system at freestream Mach numbers of 0.4 and 0.6. They concluded that the convection speed ratio of the nodal disturbances is a function of frequency and that the upstream-travelling wave was acoustic in nature.

The complexity of cavity flows makes it very difficult to have a simple yet comprehensive analytic model. But numerical and computational work in the past has met with varying degrees of success. Recent work in simulation of cavity flows has been reported by Amit Basu et.al [25], Majdalani [26] and others.

## 2.3 Important Parameters

Important parameters characterizing cavity flows are

### Upstream Boundary Layer & Freestream Parameters

Boundary layer thickness ( $\delta$ )

Momentum thickness ( $\theta$ )

Freestream velocity ( $U_\infty$ )

Mach number ( $M$ )

### Free Shear layer parameters

Hydrodynamic wavelength ( $\lambda$ )

Convective velocity ( $U_c$ )

Shear layer Frequency ( $f$ )

Shear layer momentum thickness ( $\theta(x)$ )

Shear layer growth rate ( $d\theta / dx$ )

Velocity profile ( $U(x)$ )

### Cavity Geometry Parameters

Cavity length ( $L$ )

Cavity depth ( $D$ )

Cavity width ( $W$ )

### Acoustic Radiation Parameters

Acoustic wavelength ( $\lambda_a$ )

Speed of sound ( $c$ )

Acoustic frequency ( $f_a$ )

RMS pressure at base of cavity ( $P_b$ )

RMS pressure at cavity opening ( $P_o$ )

Figure 2-6 shows important parameters pertinent to cavity flows.

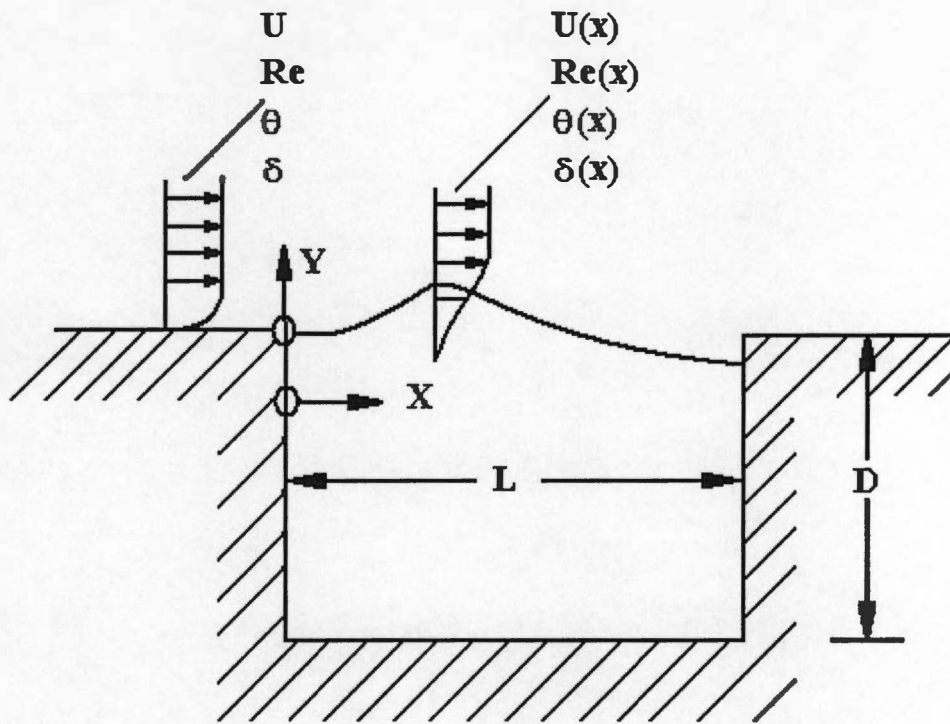


Figure 2 – 6. Important parameters in cavity oscillations

## *Chapter 3*

### **Experimental Approach**

#### **3.1 Wind Tunnel**

All experiments were conducted in the UTSI low speed wind tunnel. This is an open circuit, closed test section, continuous wind tunnel. The tunnel operates in in-draft mode. The electric fan installed downstream of the test section sucks the air through a contoured bell-mouth for maximum flow uniformity. A variable frequency controller operates the fan to achieve continuous tunnel flow speed adjustments. The constant test section is 20 in. (50.8 cm) wide by 14 in. (35.6 cm) high and has a length of 42.1 in. (107 cm). Optical access for the camera and laser sheet is provided in the side door and roof of the test section respectively. The tunnel is capable of operating at speeds ranging from 05 m/s to 65m/s.

#### **3.2 Cavity Model**

A flat plate with a rectangular, three dimensional cavity was designed, manufactured and mounted in the test section as shown in figure 3-1 and 3-2. The plate was 25.0 in. long, 6.5 in. wide and 1.0 in. thick. It has a 0.5 in. long elliptic and 6.5 in. wedge-shaped leading edge contour to avoid separation and have a fully developed boundary layer at the leading edge of the cavity. The trailing edge had a 4.5 in. wedge-shaped contour to minimize effects due to

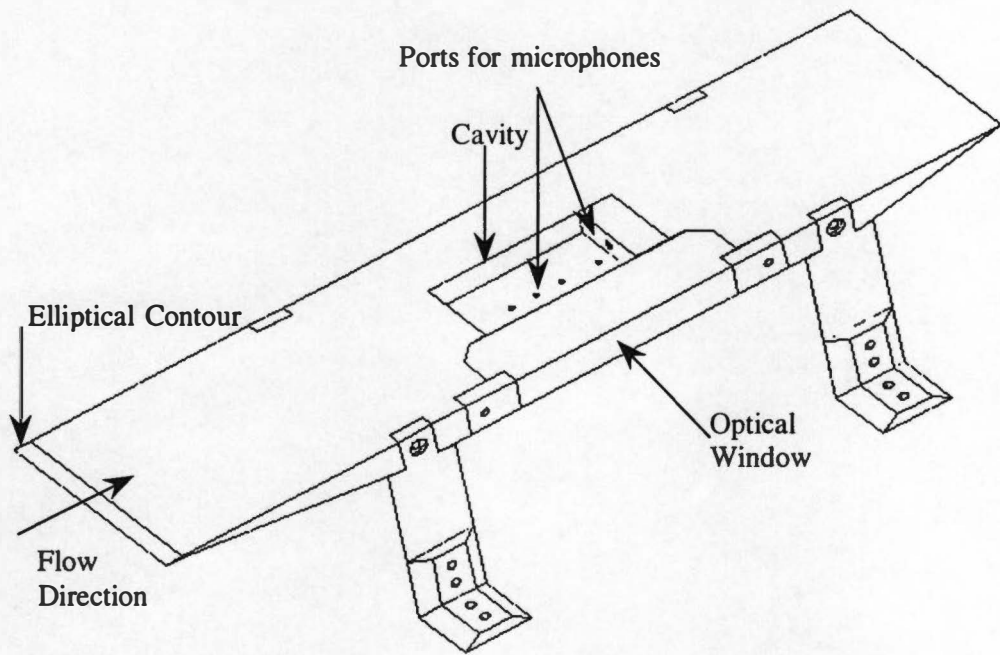


Figure 3 – 1. Cavity Model installed in UTSI low speed wind tunnel



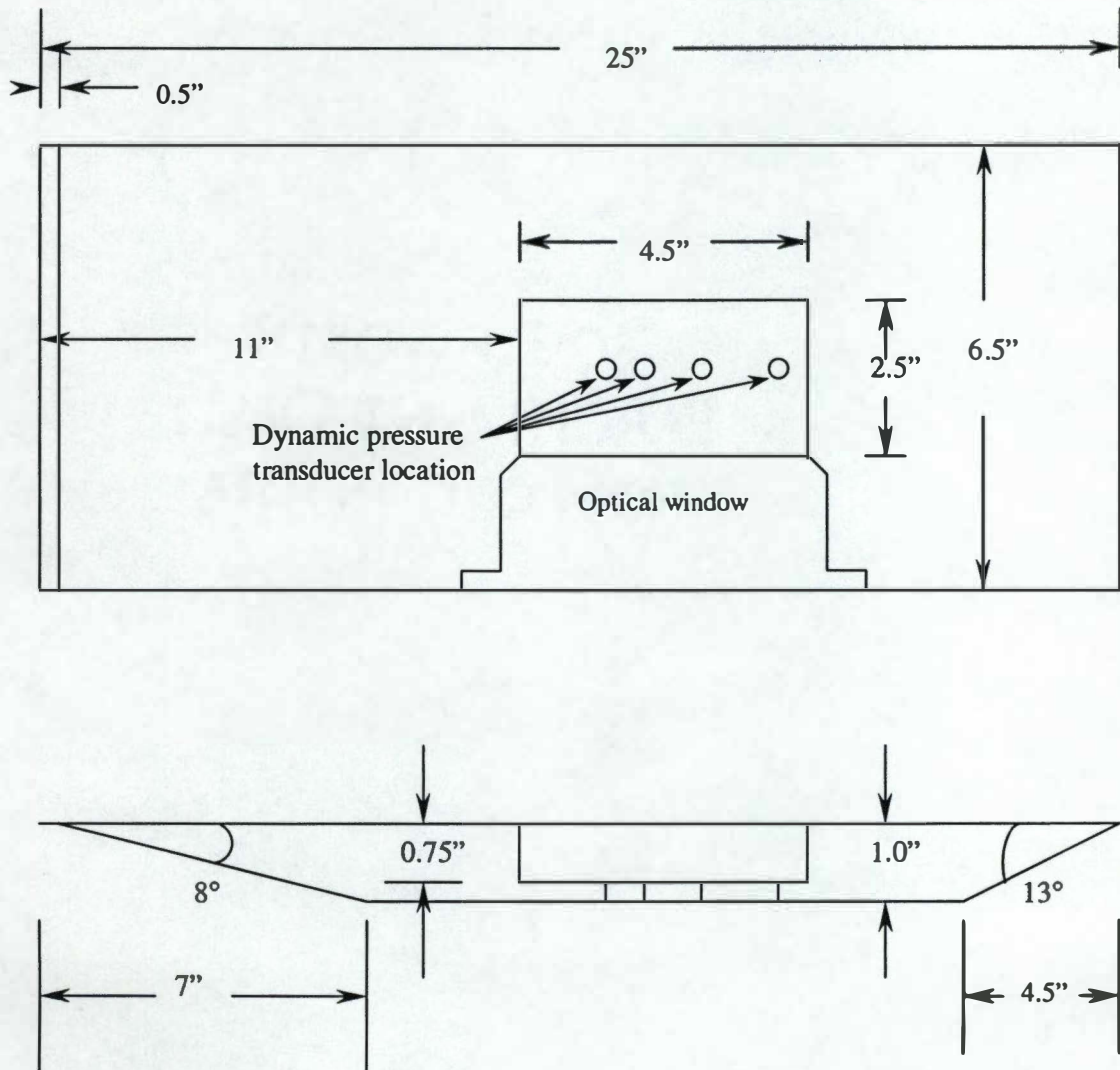


Figure 3 – 2. Cavity model layout ( All dimensions in inches )

separation. Four legs on the sides of the plate supported the model. The legs were contoured to minimize tunnel blockage and to reduce flow separation. The cavity was located 11 in. aft of the leading edge of the flat plate. The maximum dimensions of the cavity are 4.5 in. long, 0.75 in. deep and 2.5 in. wide. Different  $L/D$  ratios (6.0, 4.5, 3.5, 2.67 and 2.0) were achieved by placing blocks of varying sizes inside the cavity while keeping the depth and width unchanged. The leading edge of the cavity remained fixed for a Reynolds number for each speed. The cavity had a width to depth ratio of 3.33. A Plexiglas window (6.5" length x 2" width x 1" thick) on one side of the cavity which was specially designed to allow optical access inside the cavity. The blockage ratio of the model was less than 5% and is below acceptable limits for low speed subsonic flows. The tests were conducted at speeds ranging from 55 ft/sec to 214 ft/sec and Reynolds number ranging from 300,000 to 1,200,000.

### **3.3 Instrumentation and Data Acquisition**

#### **3.3.1 Pressure Measurement System**

Figure 3-3 shows the dynamic pressure transducers layout. For most  $L/D$  ratios two microphones were used, one on the cavity floor near the trailing edge and one on the trailing edge wall. For larger  $L/D$  ratios of 3.5 and 4.5 an additional microphone was placed on the cavity floor near the leading edge. The microphones used were Bruel & Kjaer® Type 4136. Each microphone had a diameter of ¼ inch. The microphones had a sensitivity of 1.6 mV/Pa and had a flat response in the frequency range of 4Hz to 70 kHz. The microphones had a dynamic range of 47 to 172 dB when connected with Bruel & Kjaer® preamplifier Type 2670. Preamplifier type 2670 had an operational frequency range of 3Hz to 200kHz and a typical attenuation of 0.25 dB. The microphones were powered by Bruel & Kjaer® Multiplexer Type 2822, which had differential outputs to avoid ground loops.

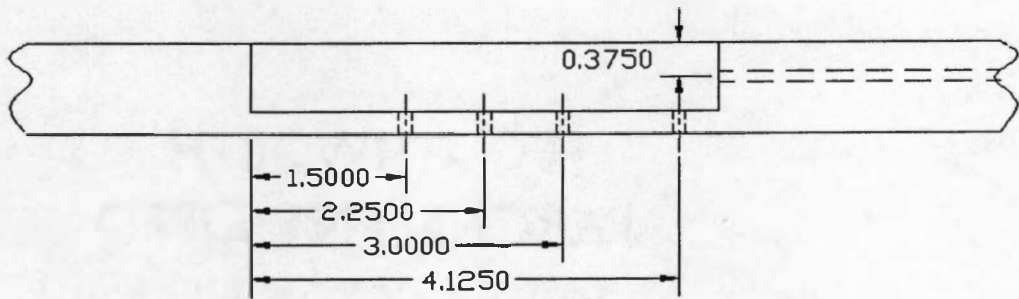


Figure 3 – 3. Cavity instrumentation layout showing the positions where microphones were used to make measurement of pressures

It had twelve channels and a frequency response of 2Hz to 200Hz ( $\pm 0.3$  dB). The outputs of the multiplexer were connected to the digital data acquisition hardware IOTECH<sup>®</sup> WAVEBOOK/512 system. This system consisted of a 8-channel, 12-bit resolution, 1MHz sampling rate A/D board. It also included the Wave View software. This setup and acquisition system allowed one to configure, display and save data to disk. The WBK20 PC-Card/EPP (enhanced parallel port) interface card and cable was incorporated in the WAVEBOOK/512 for an enhanced rate of data transfer between the data acquisition system and the computer connected to it. Data from the microphones was recorded at a sampling rate of 10000Hz giving a frequency range of 0 - 5000Hz. 8192 data points were taken for each condition. They were divided into 8 blocks of 1024 points and a Fourier analysis was performed on the data using a Hanning Window to give the frequency domain. The power spectrum was obtained from this.

### 3.3.2 Particle image velocimetry (PIV) System

The PIV technique is based on the fundamental definition of velocity

$$u(x, t) = \frac{\Delta x(x, t)}{\Delta t}$$

where  $\Delta x$  is the displacement of a marker (seeds), located at 'x' at a time 't', over a short interval  $\Delta t$  separating observations of the marker images. This Lagrangian velocity of the marker is equated to the Eulerian velocity at that location. The accuracy of the measurements depends on how accurately the seeds follow the flow. PIV is performed by illuminating a seeded flow field with a planar laser sheet, which is pulsed at a known time interval forming one or more images of each seed particle. The elapsed time between each exposure of the seed particles is accurately recorded. This technique has the ability to collect non-intrusive data

over large spatial grids. This ability to perform spatial flow field studies enables PIV to identify instantaneous flow structures and compute spatial quantities such as vorticity and the instantaneous contribution of the Reynolds stress which are almost impossible to obtain in point based techniques.

In this study, a continuum Nd:YAG laser was used to provide a thin planar laser sheet. It provides an output pulse energy of 200 mJ/pulse at a wavelength of 532 nm (green light). The horizontally and vertically polarized beams of the two lasers are combined by a polarized beam splitter, then shaped by spherical and cylindrical lenses to form a planar beam profile with thickness about 1 mm and width 50 to 100 mm. TSI®'s PIVCAM 10-30 CCD camera with a 60 mm FL F/2.8 Micro Nikkor Lens was used for image capture. It has 1,026,144 light sensitive pixels and is capable of taking 30 frames per second. Since an image pair is required to get a single velocity field, the effective sampling rate of the flow was 15 Hz. TSI® Model 610032 Laser pulse synchronizer controls the camera and the laser. External triggering is also possible. The synchronizer is connected to a 233 MHz personal computer loaded with TSI®'s Insight® software. This is a simple graphic user interface, which allows the operator to easily define all laser, camera and data recording options. The Insight® software allows for image spatial domain calibration so that the calculated velocity vectors could be expressed in useful engineering units (m/s). The layout of the PIV system is shown in figure 3-4. The image spatial domain is calibrated by taking the image of a calibration scale placed over the model. The numbers of pixels between the identified points is then measured to give the calibration in terms of  $\mu\text{m}/\text{pixel}$ . The images for study were taken at a scale of 74 – 81  $\mu\text{m}/\text{pixel}$  for different L/D ratios. The optical window used in these was 2" wide. Therefore diffraction was expected. Two calibrations were done. One calibration was done inside the cavity (through the

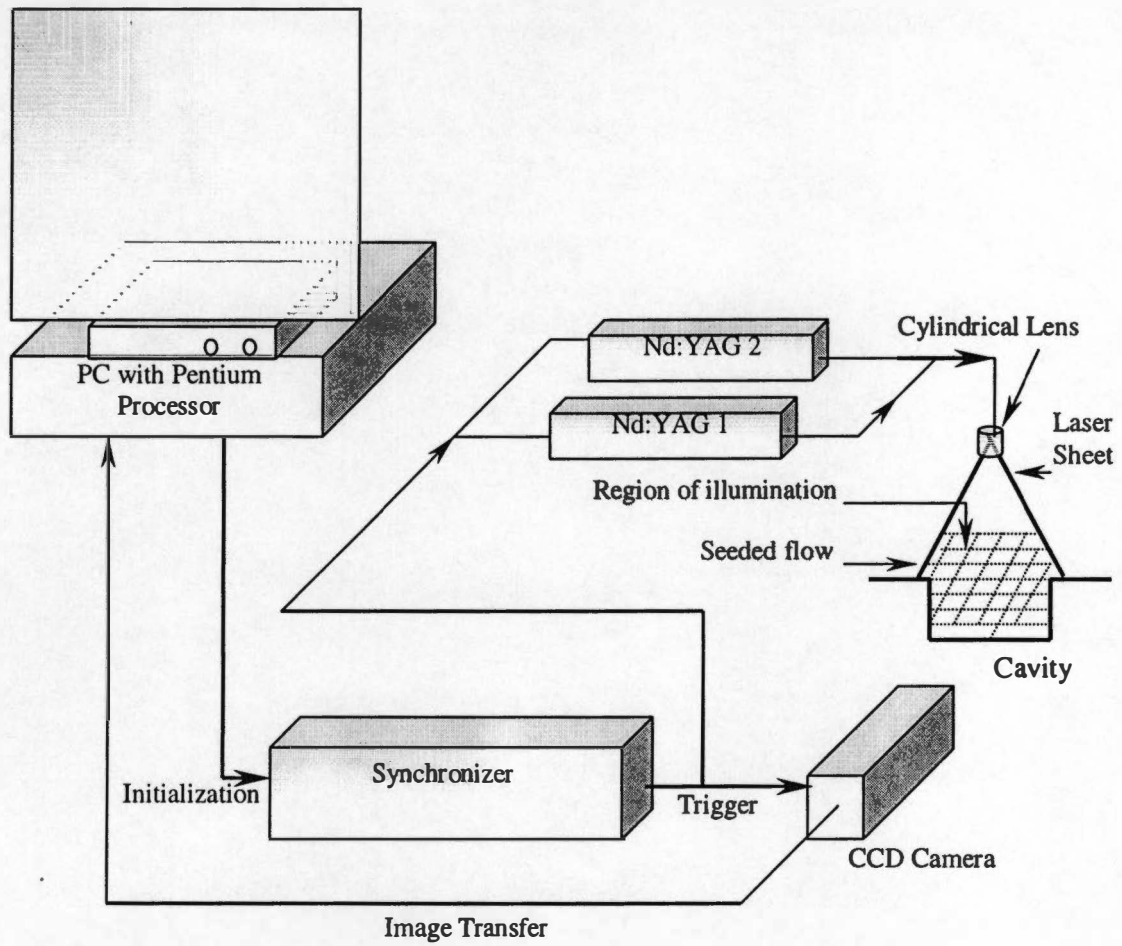


Figure 3 – 4. Schematic of the PIV System setup

optical window) and the other above the cavity. Except at the top edge of the window, the calibration results were the same. Along the edge, there was some shift in the images. The shift varied from 4 to 10 pixels along the edge. This depended on the perpendicularity between the laser sheet and the camera.

The system has the capability to take two sequential pictures within a minimum time interval of 200 nanoseconds. It uses the Frame Straddling technique to achieve such small  $\Delta T$ . The image of the seed should move less than one-fourth of the interrogation spot in the time between the first and the second laser pulses. The images for this study were taken with a  $\Delta T$  of  $3\mu\text{s}$ . The pixel displacement in the high velocity regions was in the order of 1 pixel.

As mentioned above, seeding is the most critical part for the success of PIV measurements. Smoke was used as the seeding particle. A commercial smoke generator was used to supply smoke. An aluminum box 5" x 5" x 18" settling chamber with an integrated fan assembly was placed between the exit of the smoke generator and the PVC pipe to allow uniform smoke supply. An elliptical airfoil with a series of 1/8" holes was placed in front of the model to inject smoke. The laser beam illuminated this smoke sheet.

The captured images are then processed using Insight<sup>®</sup> software. Correlation techniques are used to find the displacement of the particles. Correlation techniques generally used are auto-correlation and cross-correlation. In the auto-correlation technique, two sequential images of the seeded flow are taken in the same frame. This results in directional ambiguity, which requires image-shifting techniques to resolve. There is also a minimum time interval below which this technique cannot be used effectively. In this study, Two Frame Cross-correlation

technique was used. In this technique, two sequential images are captured in different frames and hence there is no directional ambiguity. The minimum time interval is also limited only by the ability of the camera. Figure 3-5 shows the basic difference between auto-correlation and cross-correlation. The image is divided into numerous regions called the interrogation spots. Cross-correlation allows for much smaller spot sizes. Signal to noise ratio of 2-frame cross-correlation is the best among all the correlation methods. Cross-correlation is performed in the following sequence. The 2D FFT result of image1 is multiplied by the complex conjugate of the 2D FFT result of image2. Computing the 2D FFT of the multiplication result and taking the modulus gives the correlation result. The maximum peak in the correlation plane is at the location of the movement between the two recordings. Therefore, by determining the location of the highest peak in the correlation plane, the velocity vector is found. An interrogation spot size of 64 x 64 pixels was used. The distance between any 2 vectors was 10 pixels (column-wise and row-wise) giving a resolution of about 0.75 mm. The resolution of the vector map based on the interrogation spot size is about 4.5 mm implying it can resolve structures in this order.



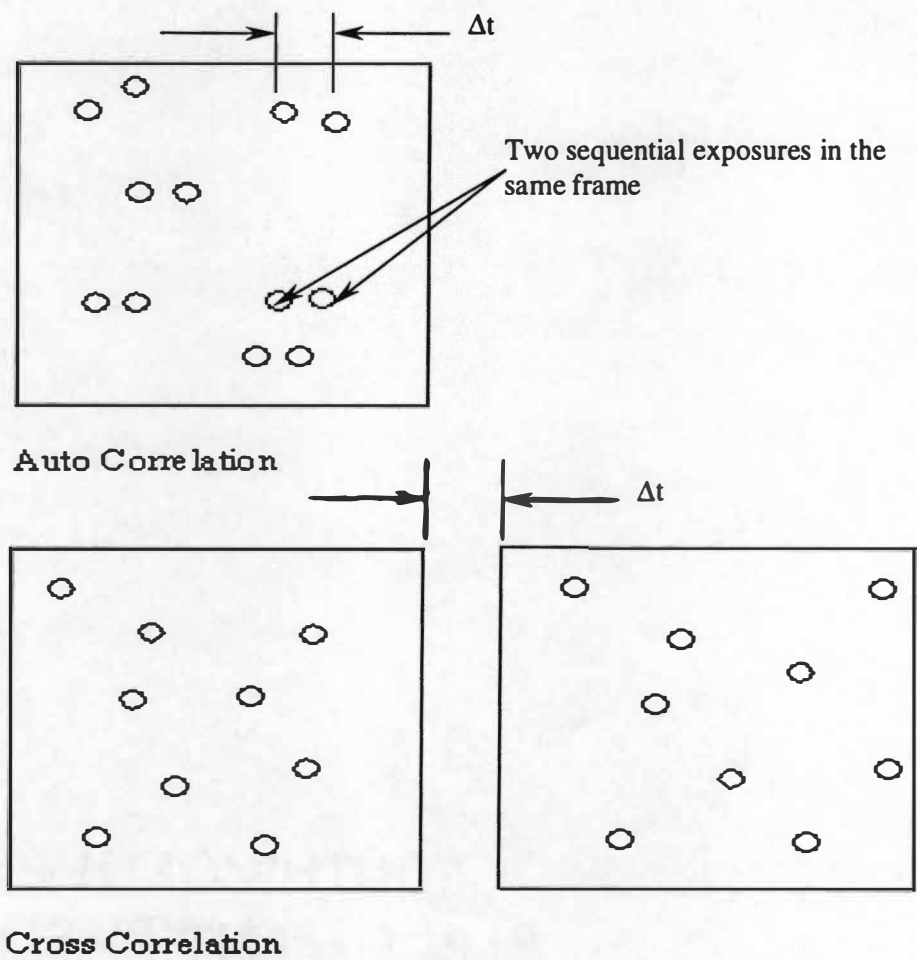


Figure 3 – 5. Correlation Techniques

## *Chapter 4*

### **Results and Discussion**

Measurements performed consisted of baseline measurements of pressure as well as PIV of the flow over the flat plate without any cavity installed. Pressure and PIV measurements with various cavities installed onto the plate at various tunnel free stream speeds were performed for selected tunnel free stream velocities. Unsteady pressure measurements were made at two distinct locations inside of each cavity, for a number of free stream velocities. One pressure measurement location was on the forward facing step and the other was located on the cavity floor just upstream of the forward facing step. The first pressure transducer was located to help directly relate the pressure traces measured to the shear layer impingement on the forward facing step. The transducer on the cavity floor was planned to measure the pressure oscillations inside of the cavity. Since different  $L/D$  ratios were achieved by placing fill-up blocks at the trailing edge, the actual position of the microphone on the cavity floor varied. The relative position of the microphone on the cavity floor from the trailing edge remained the same except for the configuration of  $L/D = 2.0$  for which the microphone was located immediately near the trailing edge.

#### **4.1 Pressure Measurements**

The base line tests were conducted without any cavity installed onto the plate. Figure 4-1 shows the acoustic spectrum for the baseline configuration at different speeds. The SPL was always below 90 dB except for a peak, which is present around 1200 Hz. Another peak of much lower amplitude is present at about 2800 Hz. The source for these peaks is the electronic

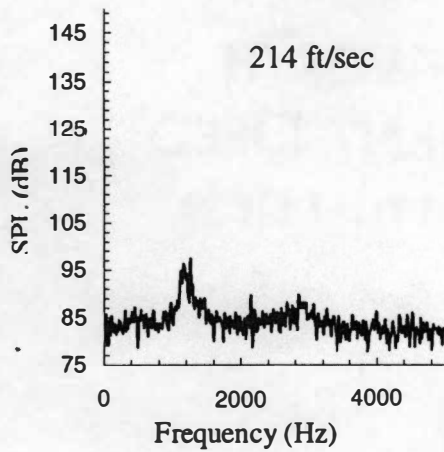
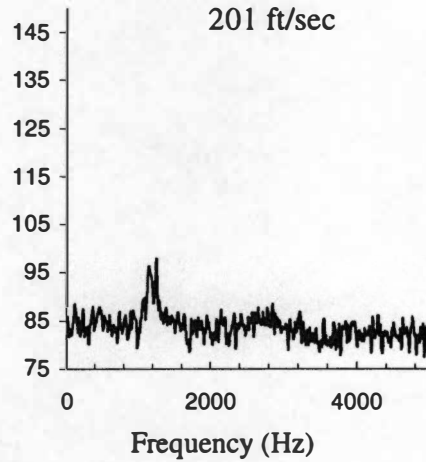
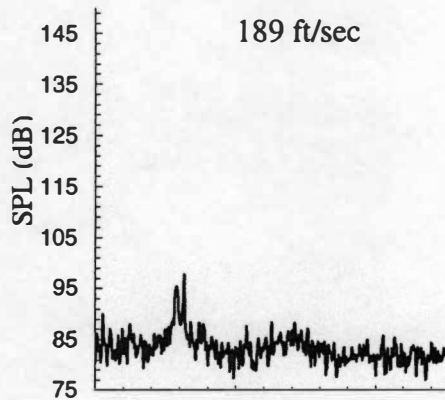
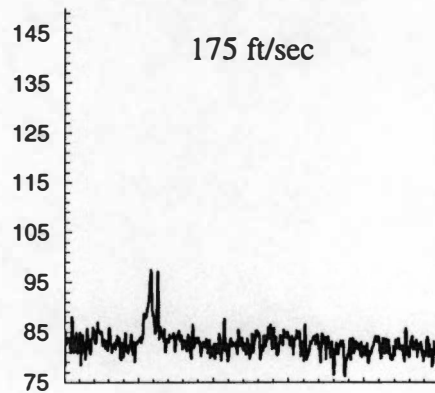
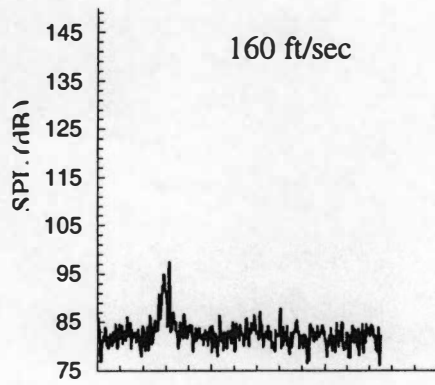


Figure 4 - 1. Baseline Power Spectrum

noise emanating from a frequency controller used to control the tunnel speed. The tunnel noise was not filtered because it didn't interfere with the cavity measurements.

Figures 4-2 to 4-5 show the power spectrum for the cavity configurations with  $L/D$  ratios 2.0, 2.67, 3.5 and 4.5 at freestream velocities of 160, 175, 189, 201 and 214 ft/sec. For all cavity configurations tested, there was a peak in the range of 120 to 240 Hz with amplitude higher than any other peak in the spectrum. These do not correspond to any of the Rossiter modes. The reason for this behavior could not be determined. Cattafesta et.al [23] also observed similar behavior. They proposed that when three Rossiter modes ( $f_c > f_b > f_a$ ) are present and satisfy the relation  $f_c - (f_a + f_b) = \Delta f \approx 0$ , significant nonlinear coupling can occur between the modes, leading to a low frequency amplitude modulation of the primary modes at  $f_m = \Delta f$  and larger than normal SPL. Even when this condition is not satisfied, the difference interactions between the primary modes namely  $(f_a' - f_a)$ ,  $(f_b' - f_b)$  and  $(f_c' - f_c)$  create a low-frequency mode that appears in the power spectrum and amplitude modulates the Rossiter modes.

Figures 4-6(a-d) show the comparison of non-dimensional frequency (Strouhal number) of the peaks and the modes predicted by Rossiter's equation for the different cavities under study. Rossiter's equation is not very accurate in predicting frequencies in the low Mach number range. The physical mechanism for this is believed to be the low levels of coherent vorticity in the shear layer at these low speeds. This results in the formation of weak and non-coherent vortices that are convected downstream to interact with the forward facing step of the cavity. As the  $L/D$  ratio increases, the coherence increases at all speeds and higher modes of oscillation are present in the cavity. This could also be possibly because of the small scale of

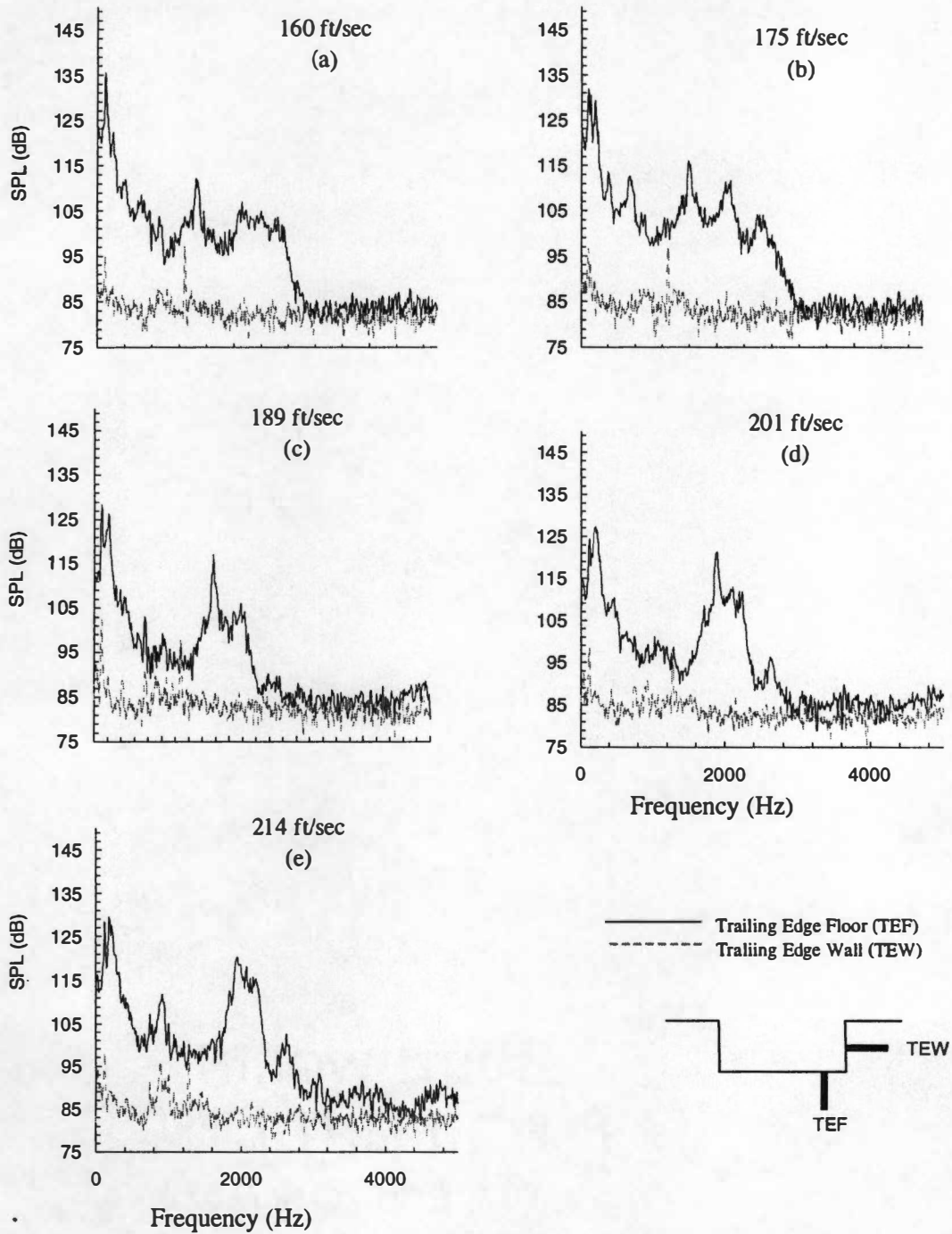


Figure 4 - 2. Power Spectrum for flow over a cavity of  $L/D = 2.0$

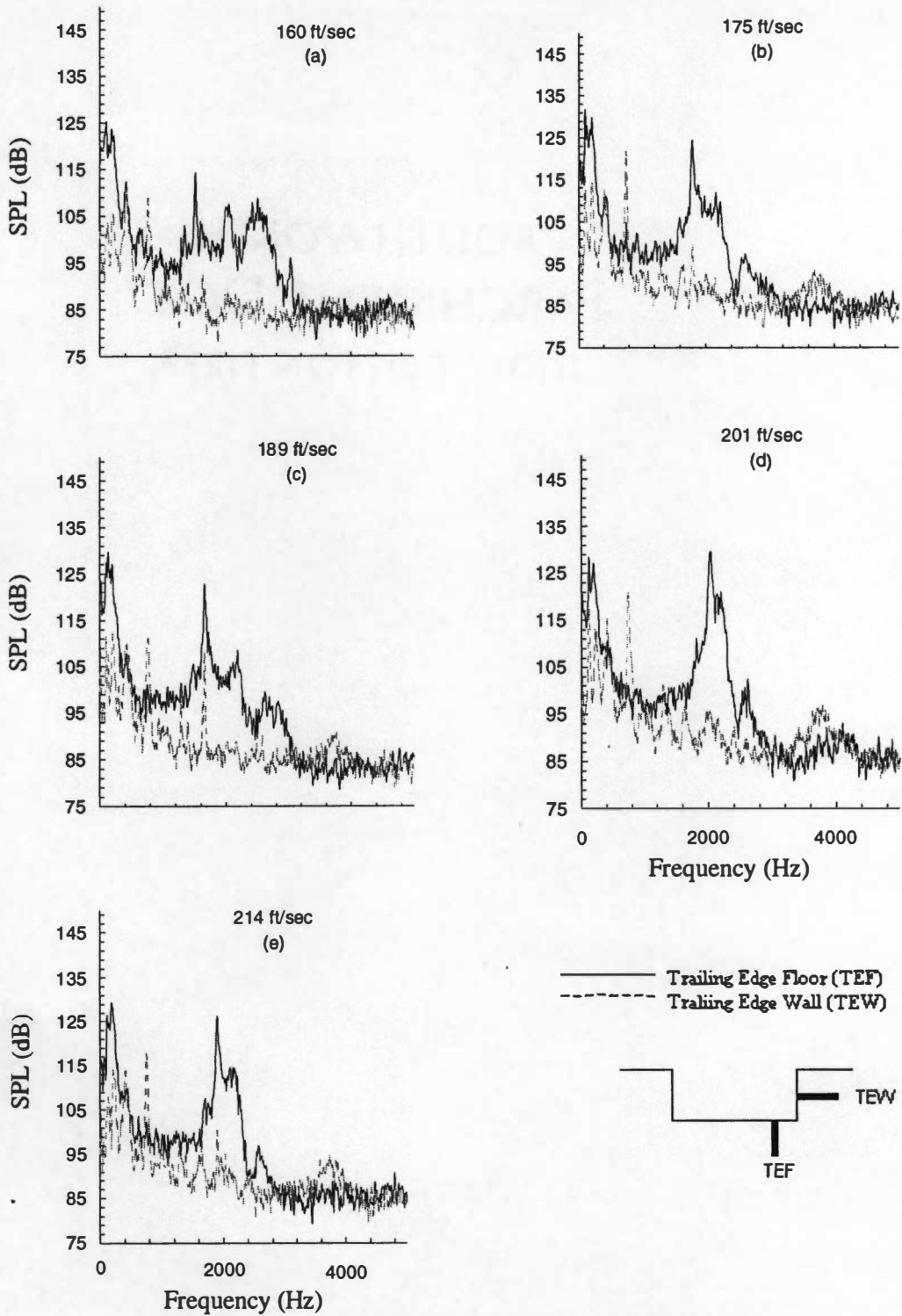


Figure 4 - 3. Power Spectrum for an L/D ratio of 2.67

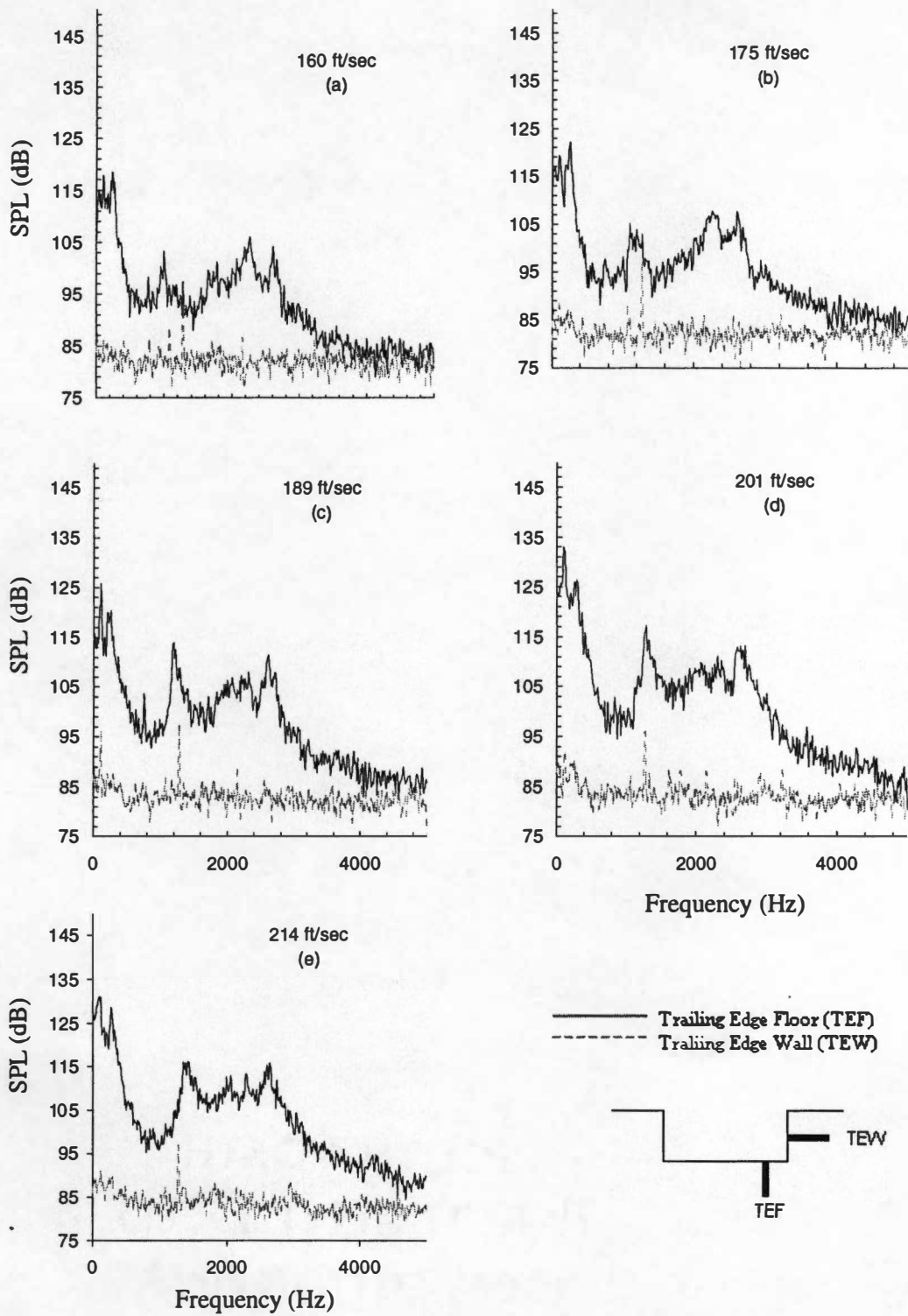


Figure 4 - 4. Power Spectrum for a cavity of L/D ratio 3.5

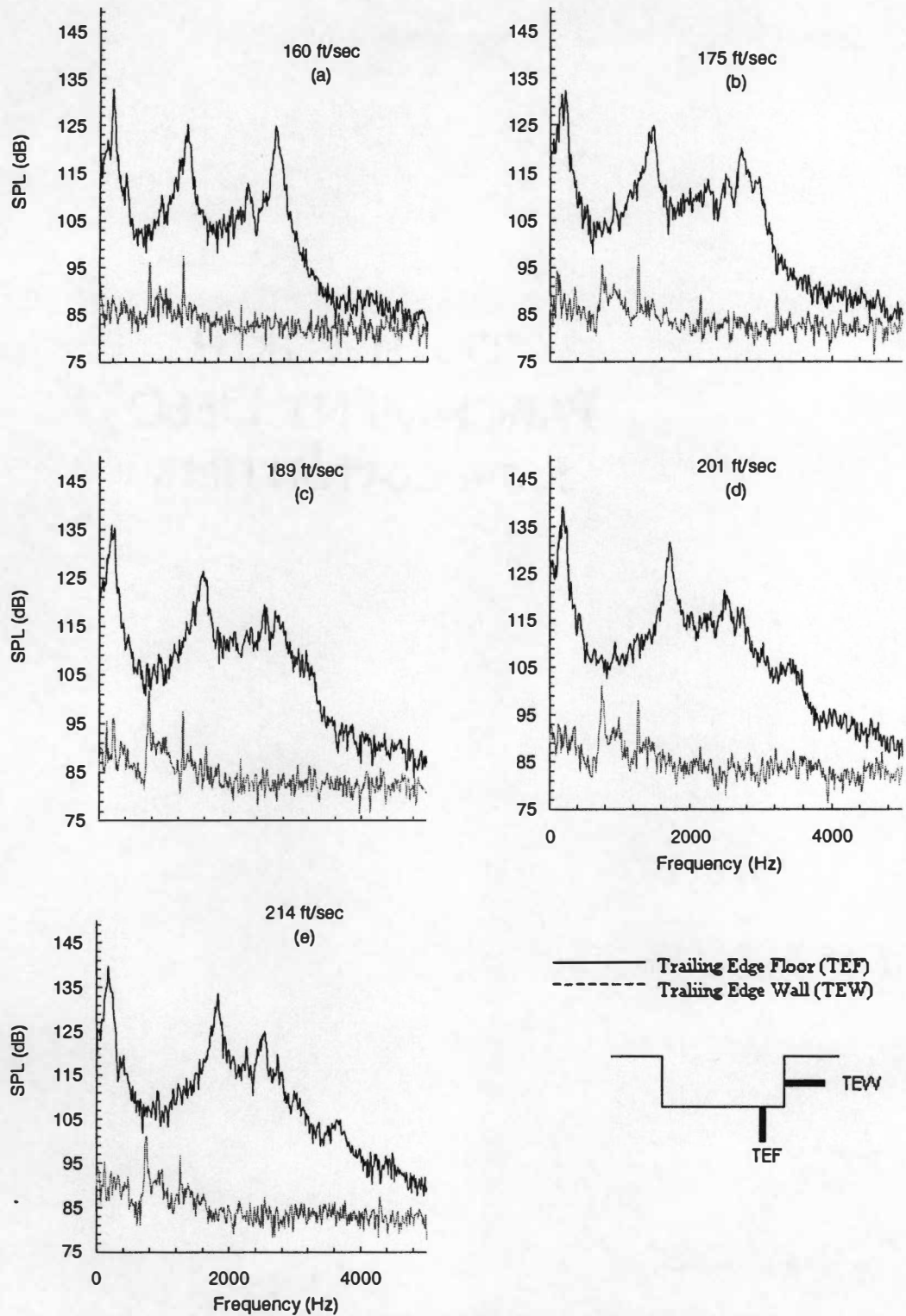


Figure 4 - 5. Power Spectrum for a cavity of L/D ratio 4.5



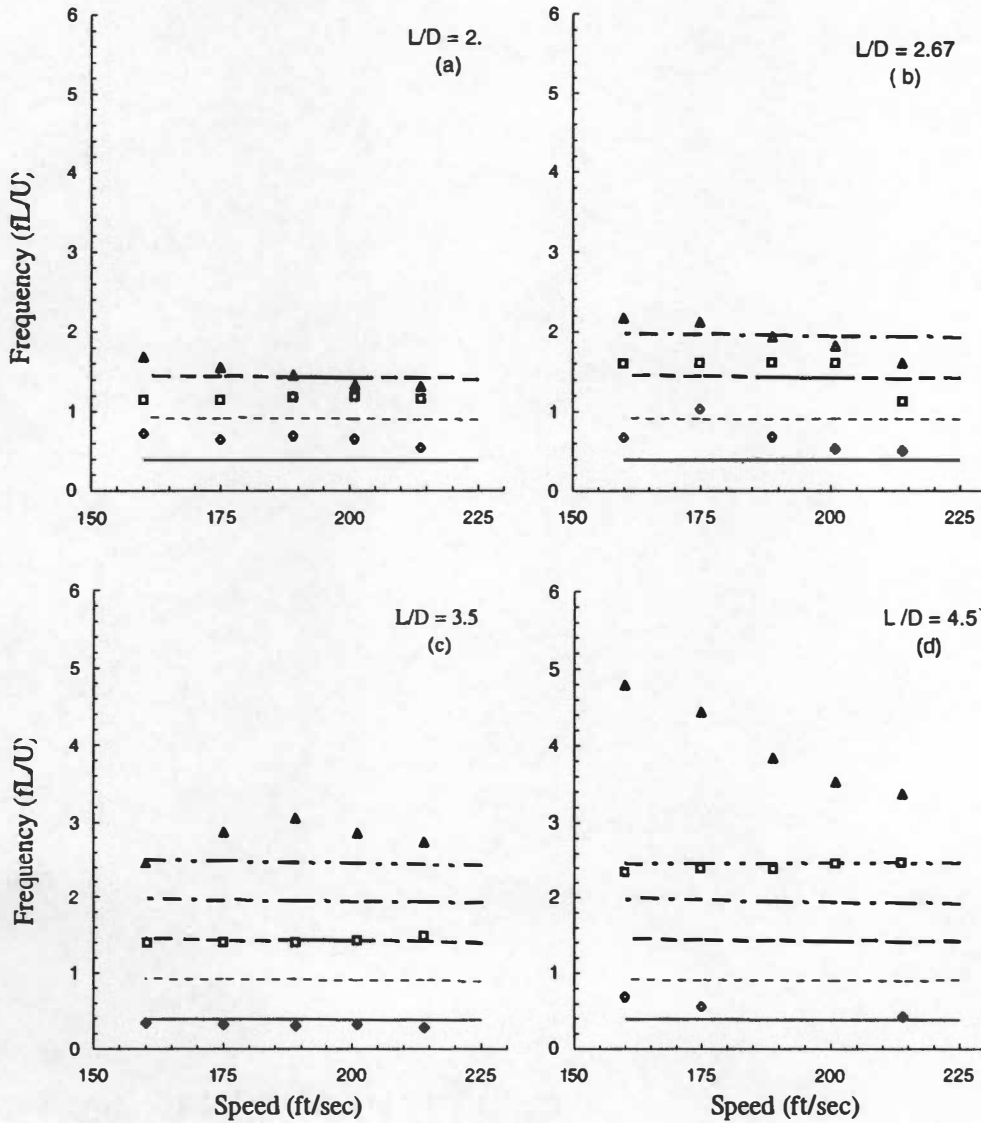
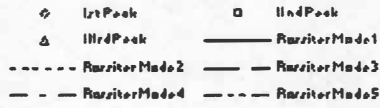


Figure 4 - 6. Comparison of Rossiter's prediction with current data

the cavity. These figures show that the cavity does indeed oscillate in the selected speed range of these tests.

Figure 4-7 shows the peak sound pressure level (SPL) in dB for each test condition. Peak amplitude is different for various speeds for a given cavity and doesn't show any regular pattern. This irregular pattern can be expected given the unsteady flow conditions and that the resonant interactions inside the cavity results in maximum amplitude peaks.

#### 4.2 Velocity Measurements

Global flow field measurements were made for flow inside and over four cavities with  $L/D$  ratios of 4.5, 3.5, 2.67 and 2.0 at speeds ranging from 55 ft/sec to 214 ft/sec. The initial step was to identify the modes of oscillation set in the cavity and to select conditions where the amplitude of the oscillation is highest. PIV measurements were then taken for these conditions. Based on the above observations, the velocity conditions of 214 ft/sec, 160 ft/sec and 55 ft/s were chosen for PIV measurements. The upstream boundary layer is an important parameter that characterizes the flow over cavities. Baseline boundary layer measurements were taken just upstream of the leading edge of the cavity. The cavity was closed for the baseline test. Due to the interference of glare from the plate surface, it was decided to use

$$\delta = y \Big|_{\frac{u}{u_\infty} = 0.95}$$

instead of the usual 0.99 position. Table 4-1 shows the boundary-layer thickness for the test conditions at about 6 mm in front of the leading edge of the cavity.

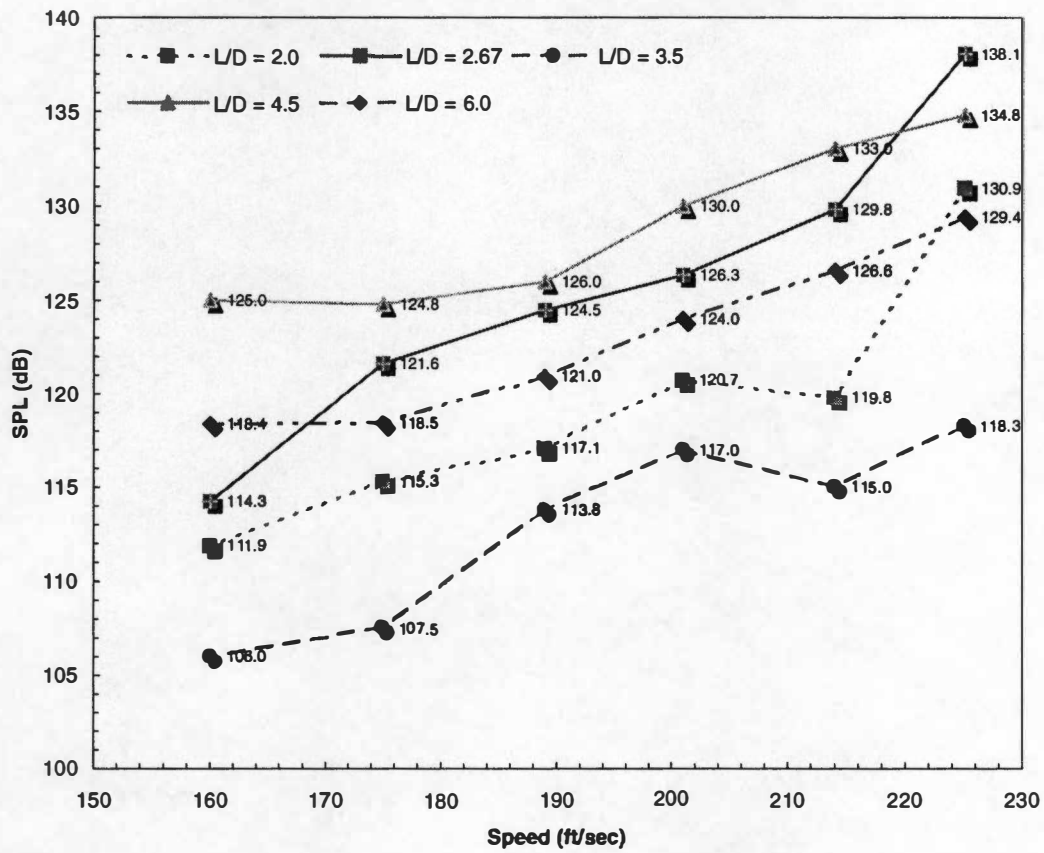


Figure 4 - 7. Peak Amplitude Vs Speed

**Table 4-1 Boundary layer thickness for the baseline test conditions  
at about 6 mm before the leading edge of the cavity**

<b>Speed (ft/sec)</b>	<b><math>\delta</math> (in.)</b>
55	0.215
160	0.315
214	0.545

Figure 4-8 shows velocity profiles for the baseline configuration without any cavity. The boundary layer profile is an average of 45 vector fields.

In the following sections, pressure spectra and PIV results for each  $L/D$  configuration will be discussed. All results presented are for a freestream velocity of 214 ft/sec. The images presented in this report were taken at random phases of the shear layer oscillation cycle (i.e., they were not taken during the same oscillation cycle and the phase relationship between any 2 images is not known). The sequence in which they are presented does not necessarily represent the sequence in which the oscillation cycle takes place. All presented images are post-processed images, which includes data-validation by a range filter, a median filter and a mean filter. The filters remove bad vectors (as in the top right hand corner of figure 4-9a.) that are mainly due to non-uniform seeding. The removed vectors were replaced by interpolation if valid vectors are available in the neighborhood. A minimal Gaussian smoothing (3 x 3) was also applied. The effects of post processing are shown in figures 4-9(a-d).

#### 4.2.1 $L/D = 2.0$

Figure 4-2e shows the pressure spectrum for the cavity of  $L/D$  ratio 2 at a freestream velocity of 214 ft/sec. The highest amplitude peak occurs at 1943 Hz and has a magnitude of 119 dB. This corresponds to Rossiter's second mode of oscillation. An instantaneous velocity vector field inside the cavity is shown in figure 4-10a. The vectors show the shear layer moving near the trailing edge and a re-circulation zone occupying the whole cavity. The streamtrace in figure 4-10b shows the re-circulation zone clearly. The velocity profiles shown at different  $x/L$  show that the thickness of the shear layer increases in the downstream direction. This increase

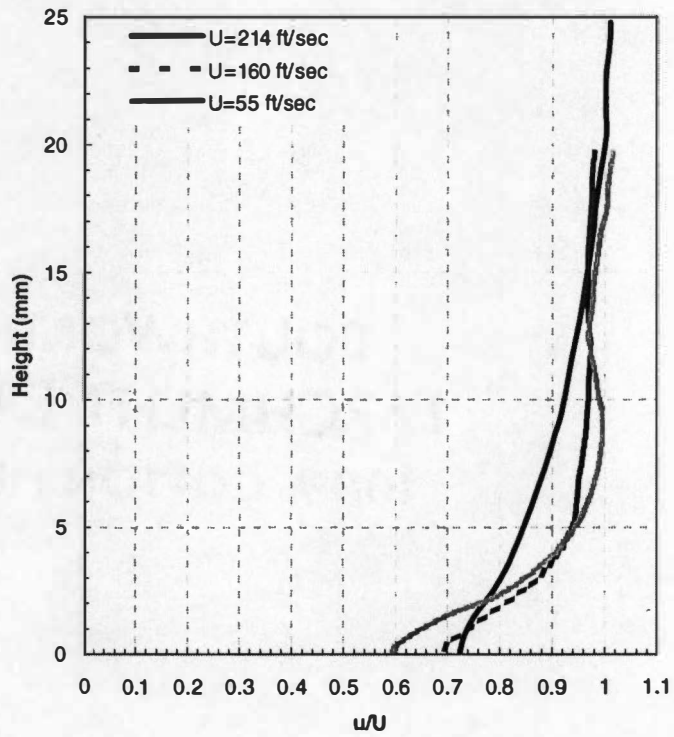
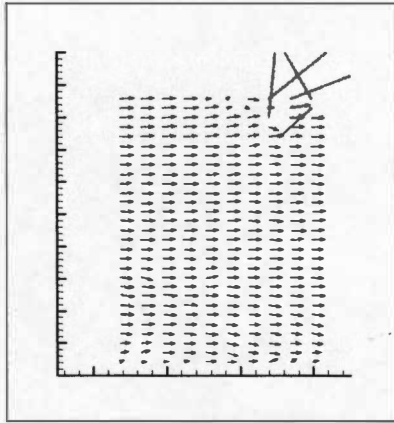
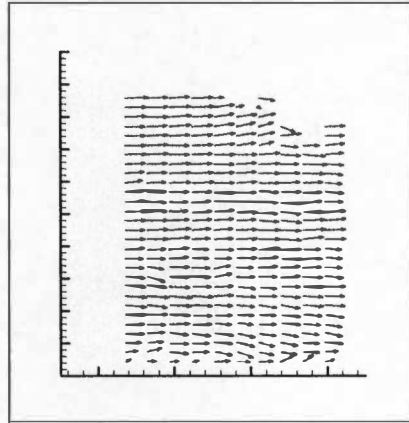


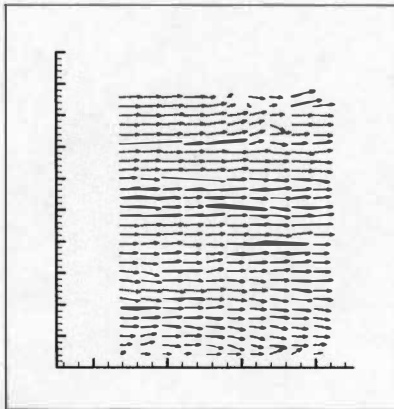
Figure 4 - 8. Baseline Boundary Layer Profiles



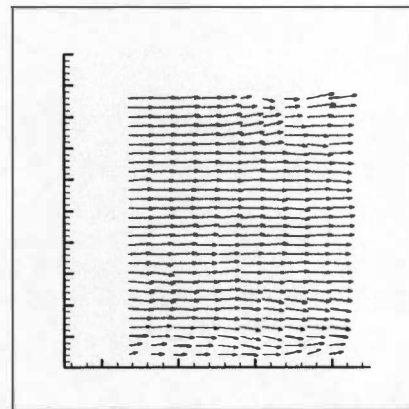
a) Raw vector image



b) After applying range & mean filter



c) After interpolation of removed vectors



d) After Gaussian smoothing (3x3)

Figure 4 - 9. Effects of postprocessing

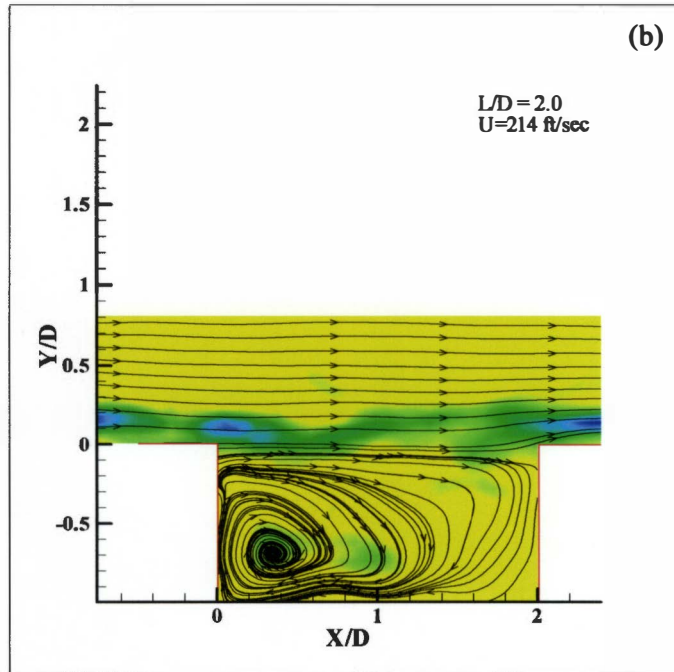
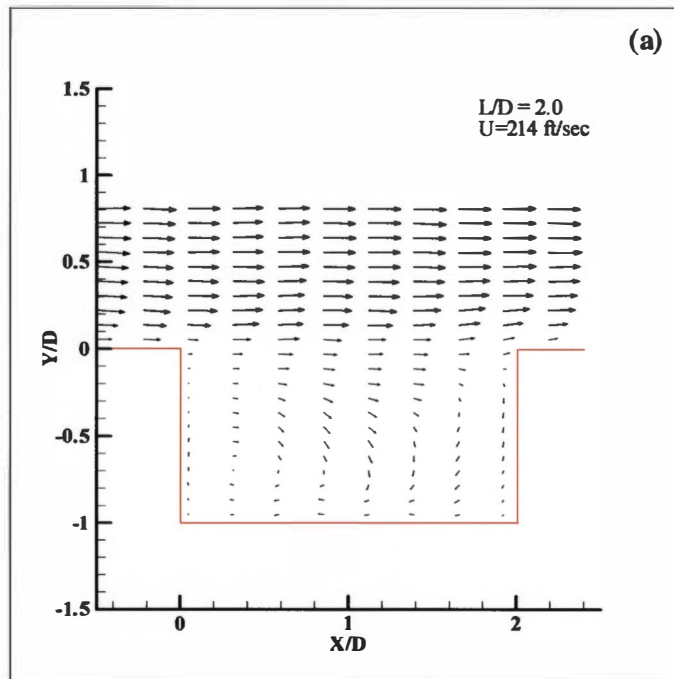


Figure 4 - 10. Mean velocity profile and streamtrace.  
(a). Velocity profile (b). Streamtrace



in shear layer thickness is attributed to the entrainment of fluid by the shear layer. The speed inside the cavity reaches up to 25% of the freestream velocity. Only a height of about 3/4" above the cavity is visible in the images. This was limited by the smoke injector's height. Comparing the sequence of images in the area above the cavity shows fluctuations in velocity up to about 20% of freestream. A possible reason could be that this is a local change in velocity because of the presence of an oscillating cavity in a subsonic flow. This could also be caused by the non-uniformity in the tunnel flow or disturbances introduced by the smoke injector in front of the model. Figure 4-11(a-e) shows the instantaneous velocity contours taken randomly. The magnitudes of velocity in the images are normalized to  $U/U_\infty$ . An animation of the velocity contour images show that the fluid layer just upstream of the leading edge oscillates. This excites the instability waves of the shear layer.

Figures 4-12(a-e) show the instantaneous vorticity contours illustrating the various stages in the oscillatory cycle. Vorticity was calculated using the relation

$$\omega = \frac{\left\{ \begin{array}{c} dv \\ dx \end{array} - \begin{array}{c} du \\ dy \end{array} \right\}}{2}$$

The presented images have reduced vorticities of the form  $\frac{\omega D}{U}$ . Contour levels range between  $\frac{\omega D}{U} = -1.2$ (blue) and  $\frac{\omega D}{U} = 0.6$ (red). The blue contour shows that vortical disturbances are present inside the shear layer. Even though the presented images were not taken during a single oscillation cycle, the presence of the discrete high vorticity regions along the shear layer indicate that the disturbances are being convected downstream. They show the

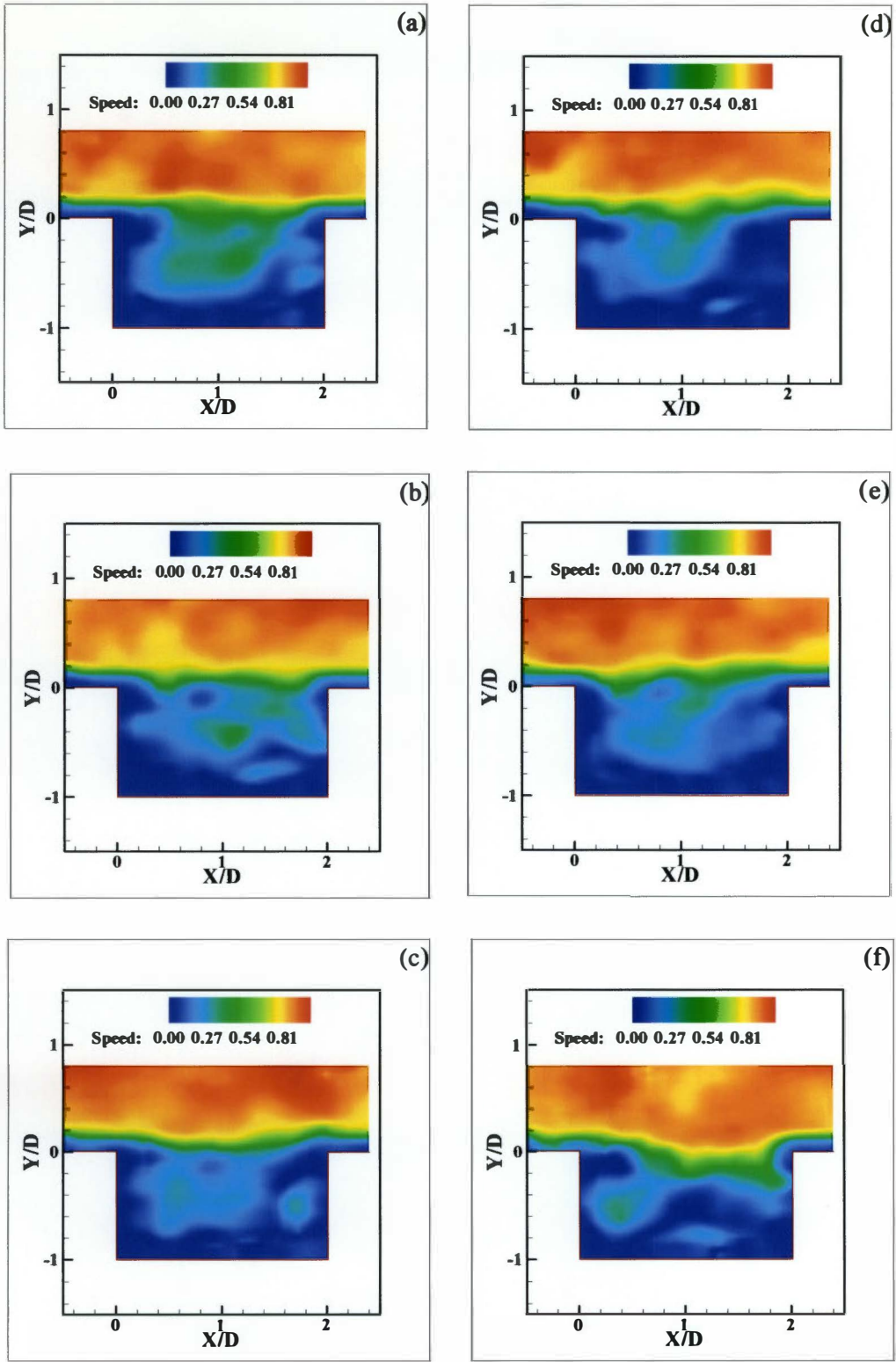


Figure 4 -11. Instantaneous Velocity Contours for flow over a cavity  
 $L/D = 2.0$  and freestream velocity = 214 ft/sec

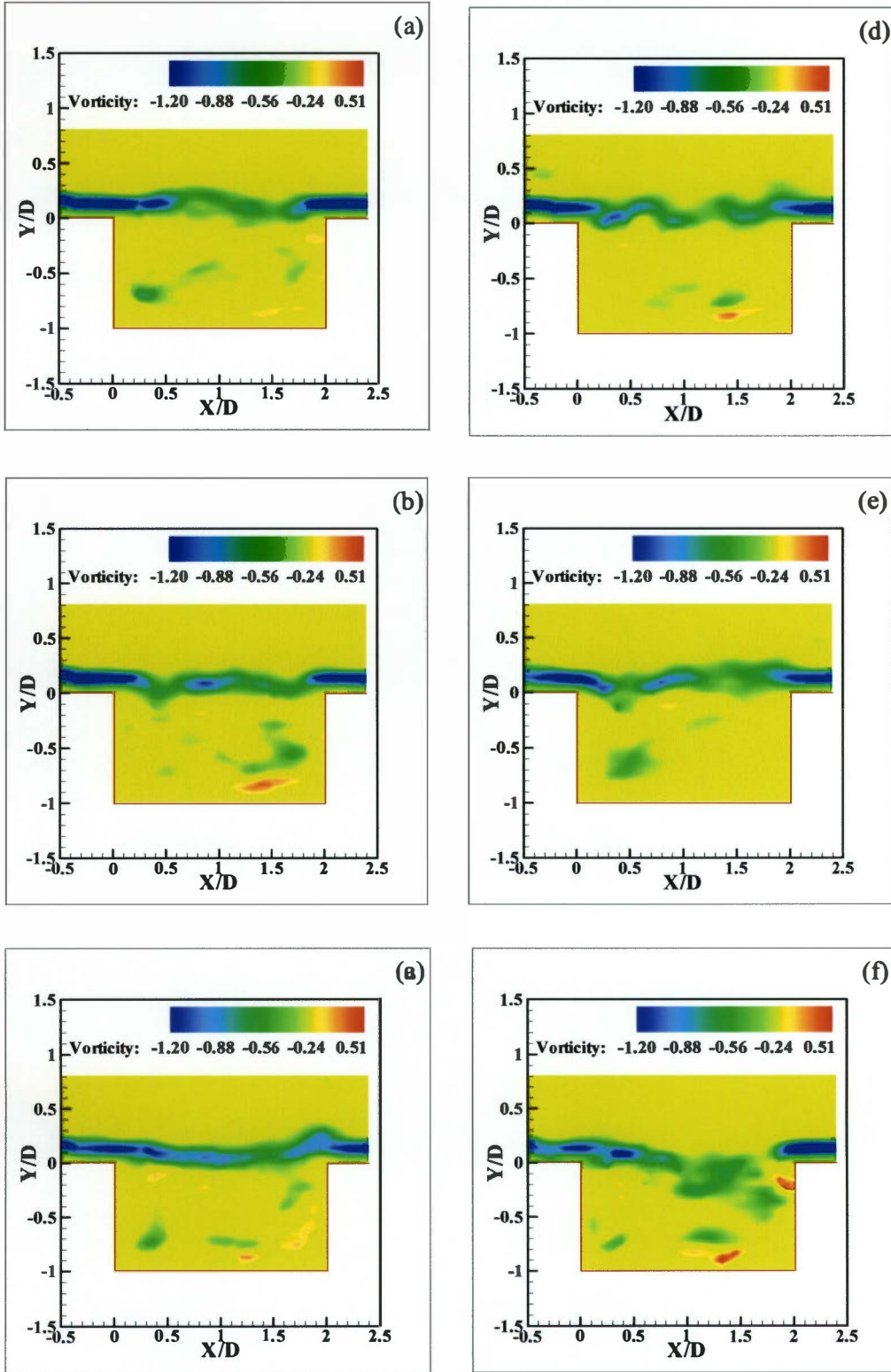


Figure 4 - 12. Instantaneous Vorticity Contours for flow over a cavity  
 $L/D = 2.0$  and freestream velocity = 214 ft/sec

shear layer oscillating near the trailing edge. Interpretation of the data near the walls has some uncertainty associated with it. The PIV images of the flow near the walls are affected by the reflected glare and hence not enough seeds are visible. These affect the boundary layer profile information; otherwise, the effect on other results is not significant.

#### **4.2.2 $L/D = 2.67$**

Figure 4-3e shows the pressure spectrum for the cavity of  $L/D$  ratio 2.67 at a freestream velocity of 214 ft/sec. The highest amplitude peak occurs at 2041 Hz and has a magnitude of 128 dB. This corresponds to Rossiter's third mode of oscillation. Figure 4-13a shows the velocity profile along the cavity length and figure 4-13b shows the mean location of vortex inside the cavity. Figures 4-14(a-e) and 4-15(a-e) show the instantaneous velocity and vorticity contours for this configuration. The flow characteristics look very similar to that of  $L/D$  ratio 2.0.

#### **4.2.3 $L/D = 3.5$**

Figure 4-4e shows the pressure spectrum for the cavity of  $L/D$  ratio 3.5 at a freestream velocity of 214 ft/sec. The highest amplitude peak occurs at 1435 Hz and has a magnitude of 115 dB. The spectrum shows a broadband excitation in the frequency range of 1400 Hz to 2600 Hz. Figure 4-16a shows the velocity profile along the cavity length and figure 4-16b shows the location of the vortex inside the cavity. Figures 4-17(a-e) and 4-18(a-e) show the instantaneous velocity and vorticity contours. The re-circulating region inside the cavity is more restricted to the rear of the cavity.

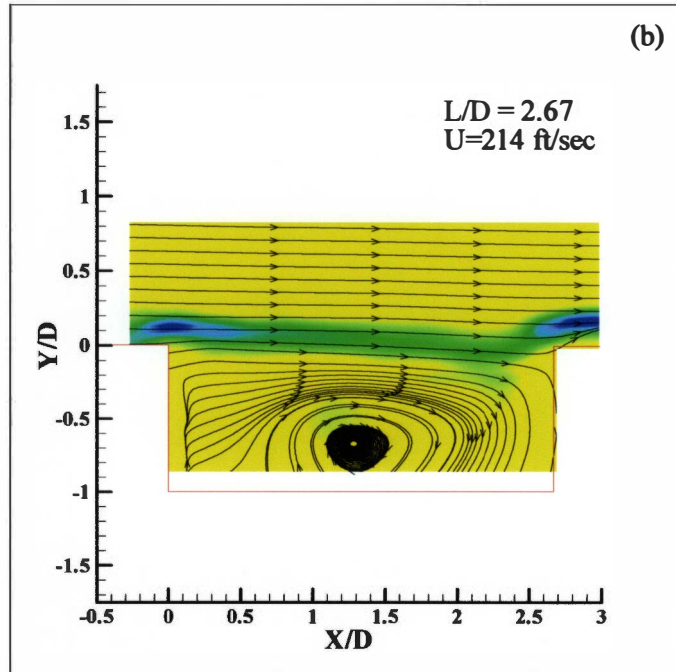
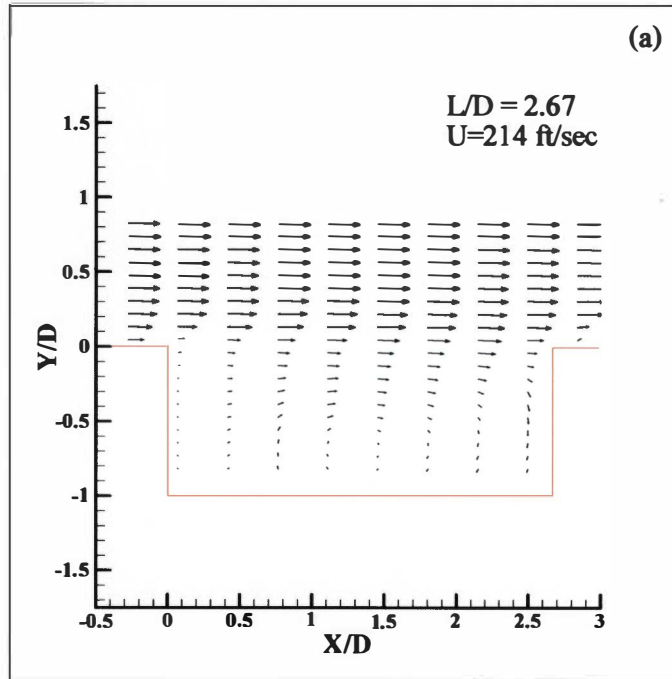


Figure 4 - 13. Mean velocity profile and streamtrace  
(a). Velocity profile (b). Streamtrace

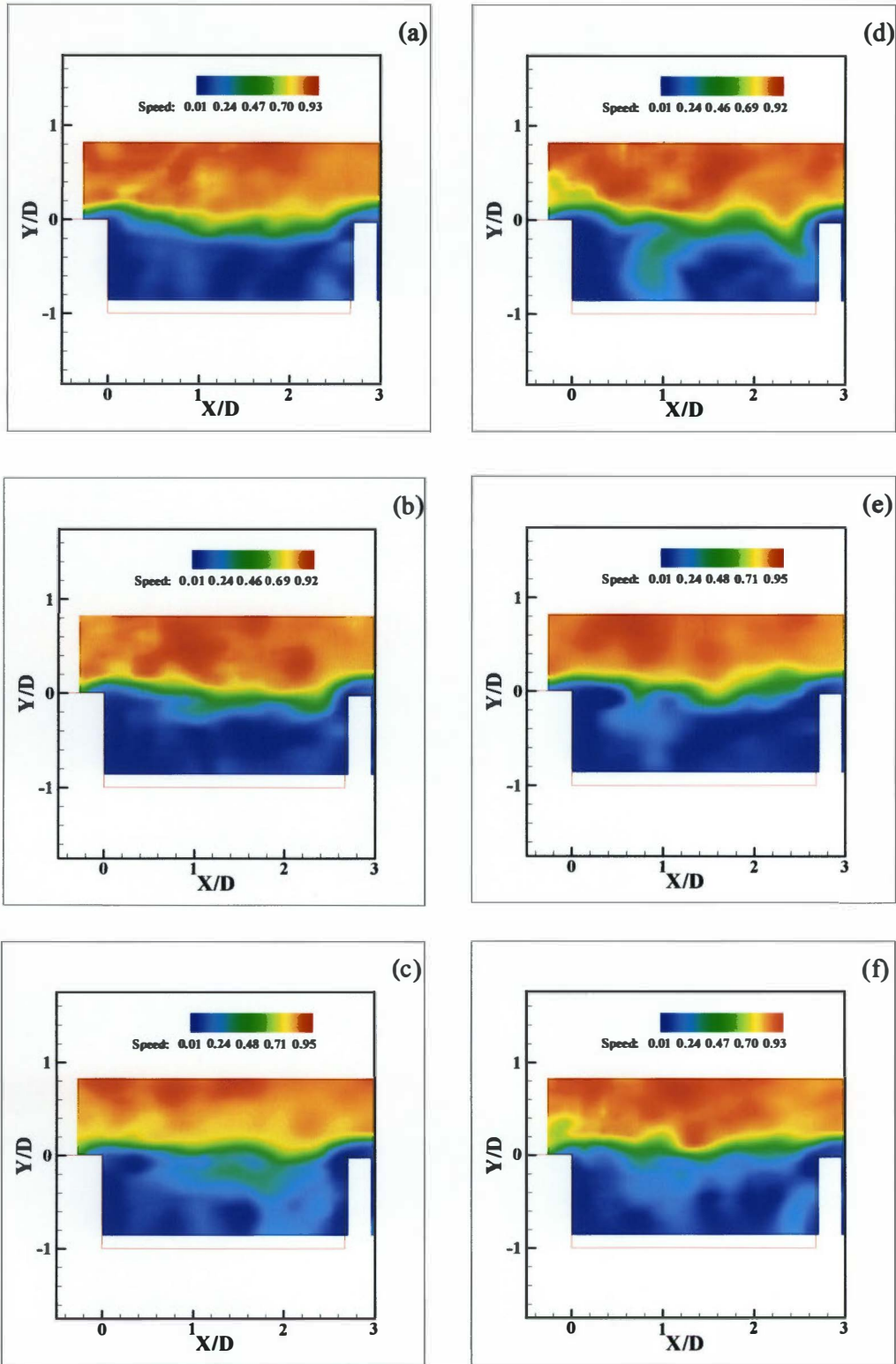


Figure 4 - 14. Instantaneous Velocity Contours for flow over a cavity  
 $L/D = 2.67$  and freestream velocity = 214 ft/sec

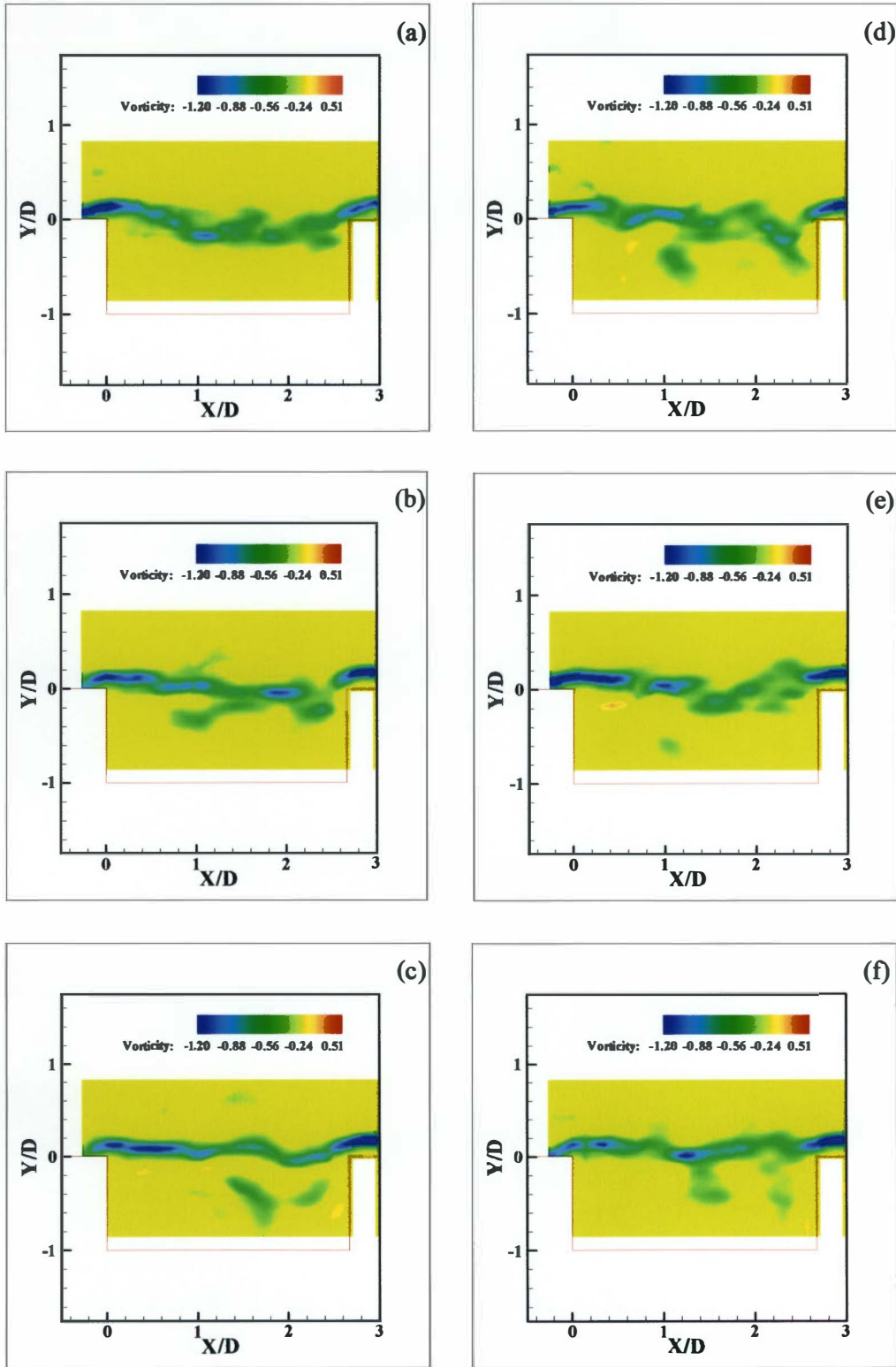


Figure 4 - 15. Instantaneous Vorticity Contours for flow over a cavity  
 $L/D = 2.67$  and freestream velocity = 214 ft/sec

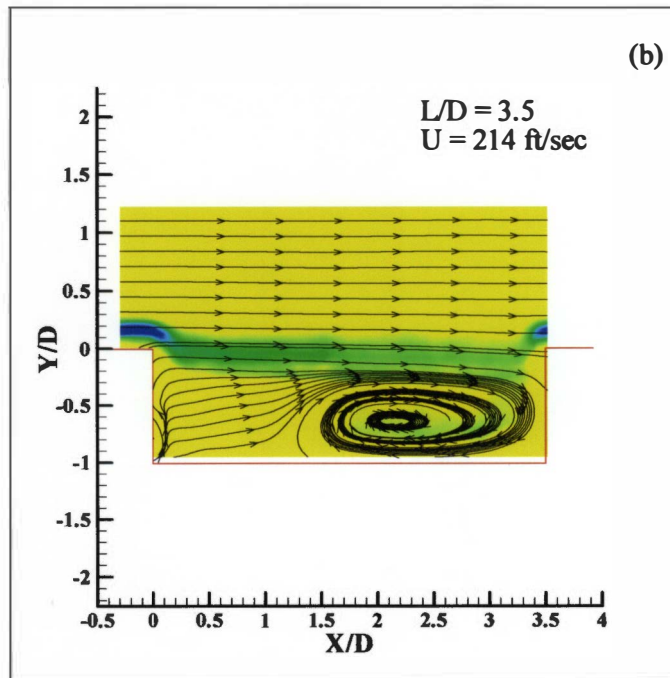
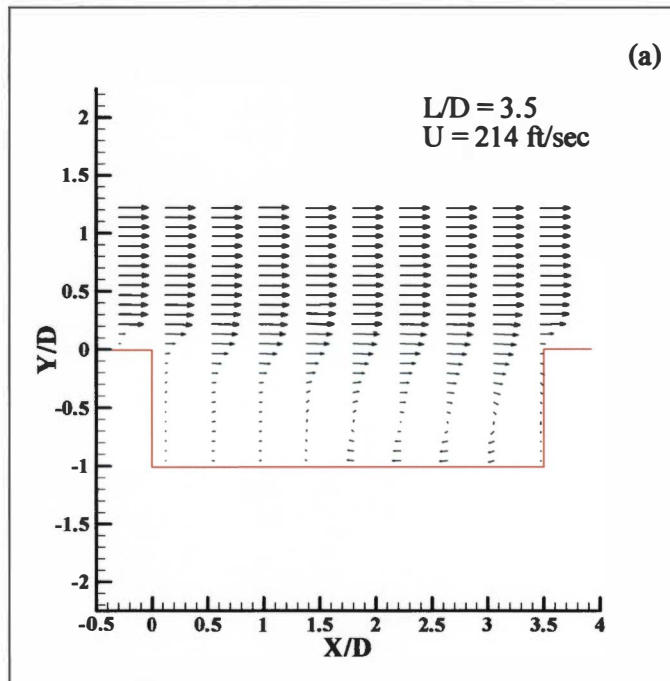


Figure 4 - 16. Mean velocity profile and streamtrace  
 (a). Velocity profile (b). Streamtrace



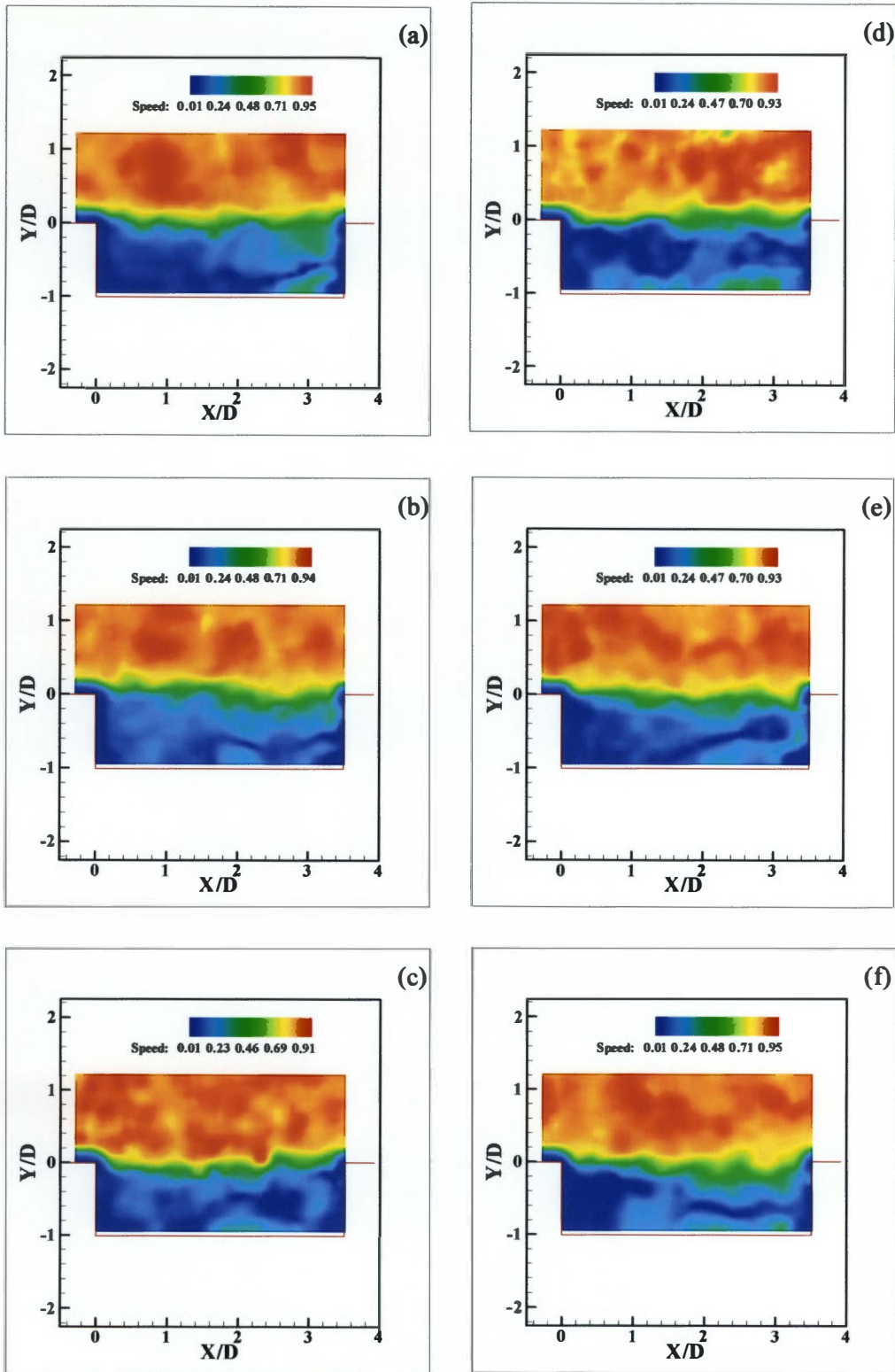


Figure 4 - 17. Instantaneous Velocity Contours for flow over a cavity  
 $L/D = 3.5$  and freestream velocity = 214 ft/sec

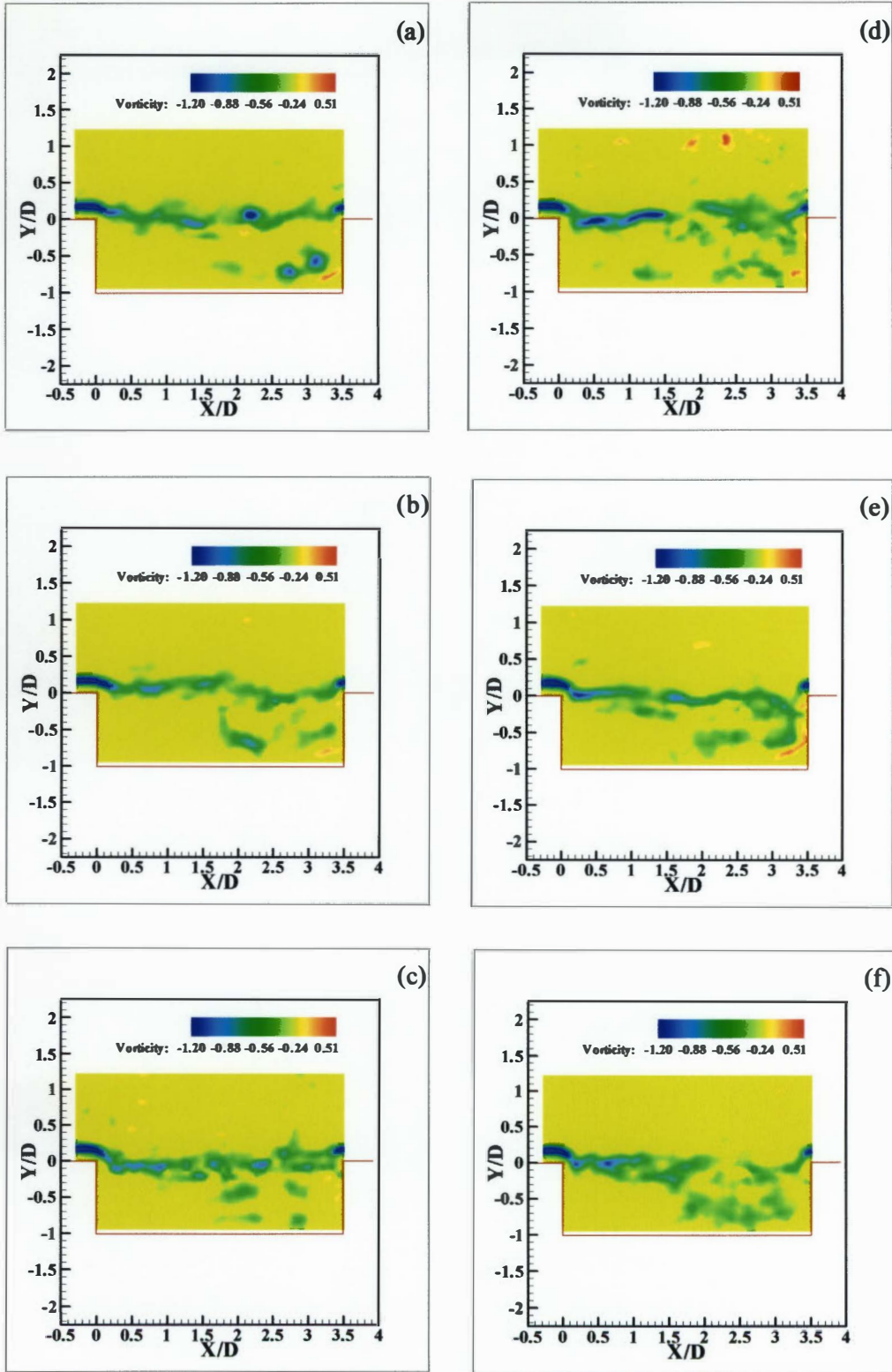


Figure 4 - 18. Instantaneous Vorticity Contours for flow over a cavity  
 $L/D = 3.5$  and freestream velocity = 214 ft/sec

#### 4.2.4 $L/D = 4.5$

Figure 4-5e shows the power spectrum for the cavity of  $L/D$  ratio 4.5 at a freestream velocity of 214 ft/sec. The highest amplitude peak occurs at 1943 Hz and has a magnitude of 133 dB. The width of the laser sheet was not large enough to cover the whole cavity. So, PIV measurements were taken in 2 halves. Figure 4-19a shows the velocity profiles along the cavity length and figure 4-19b shows the location of the vortex inside the cavity. Figures 4-20(a-e) and figures 4-21(a-e) show the instantaneous velocity and vorticity contours.

As the length to depth ratio increases, the re-circulation region near the trailing edge of the cavity seems to become stronger. The tests at lower speeds show similar results but show more disturbances in the flow. As can be expected, the amplitude of the oscillations was small because the energy available from the flow above the cavity is low because of the speed range.

Sources of error in PIV measurements include error in measurement of  $\Delta t$  and error in measurement of  $\Delta x$ .  $\Delta t$  measurements are very accurate leaving error in displacement the major source of error. Possible causes of this error include non-uniform seeding and improper choice of seeding material, glare from reflected surfaces, non-uniform intensity of the laser sheet, electronic noise during digitization, size of the interrogation spot and limitations of the peak detection techniques. In this study, the major sources of error were identified to be the glare from reflected surfaces and non-uniform seeding of the flow. Estimation of these errors is very difficult. In spite of this, the accuracy of these measurements are expected to be better than one percent.

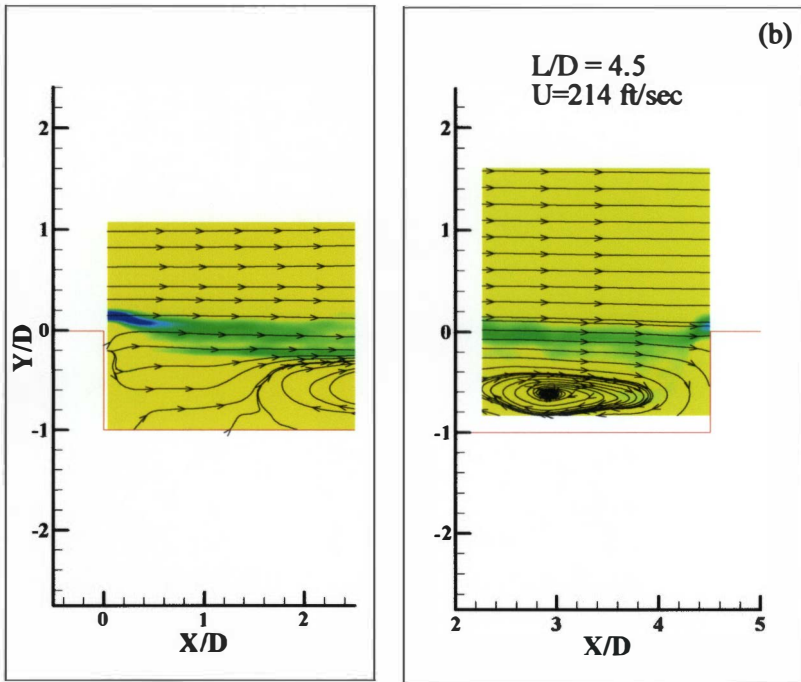
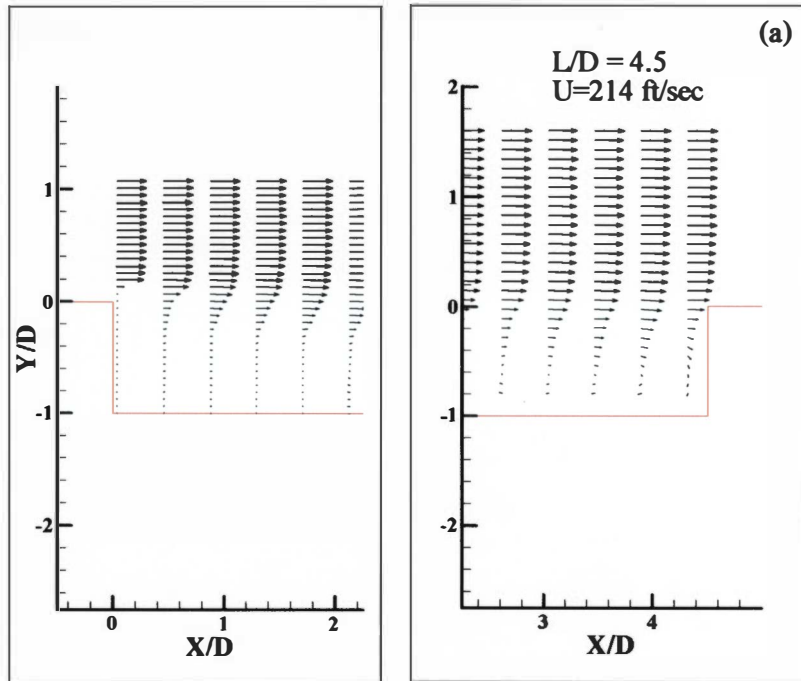


Figure 4 - 19. Mean velocity profile and streamtrace  
 (a). Velocity profile (b). Streamtrace

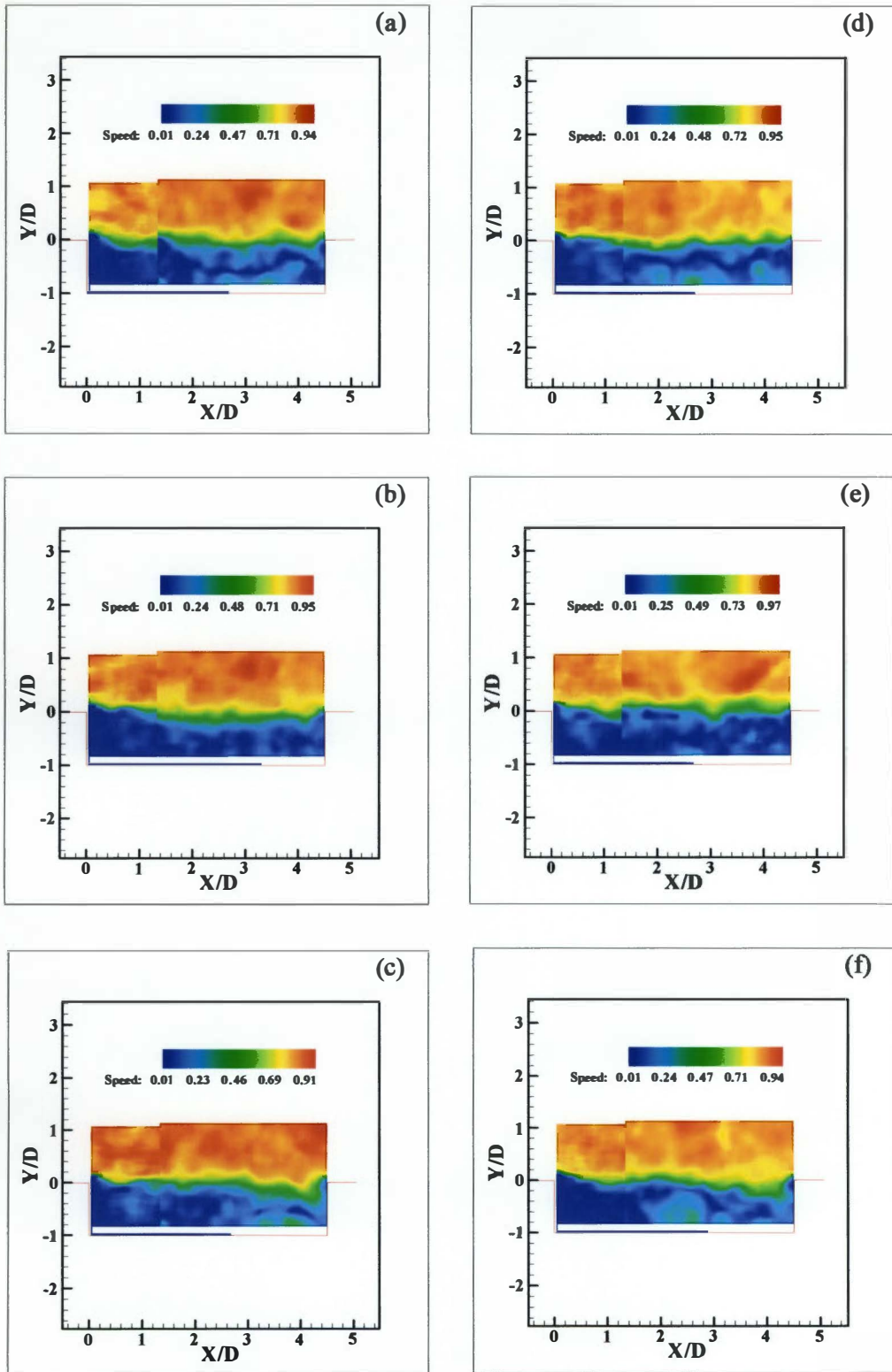


Figure 4 - 20. Instantaneous Velocity Contours for flow over a cavity  
 $L/D = 4.5$  and freestream velocity = 214 ft/sec  
 ( 2 images taken at different times are overlapped )

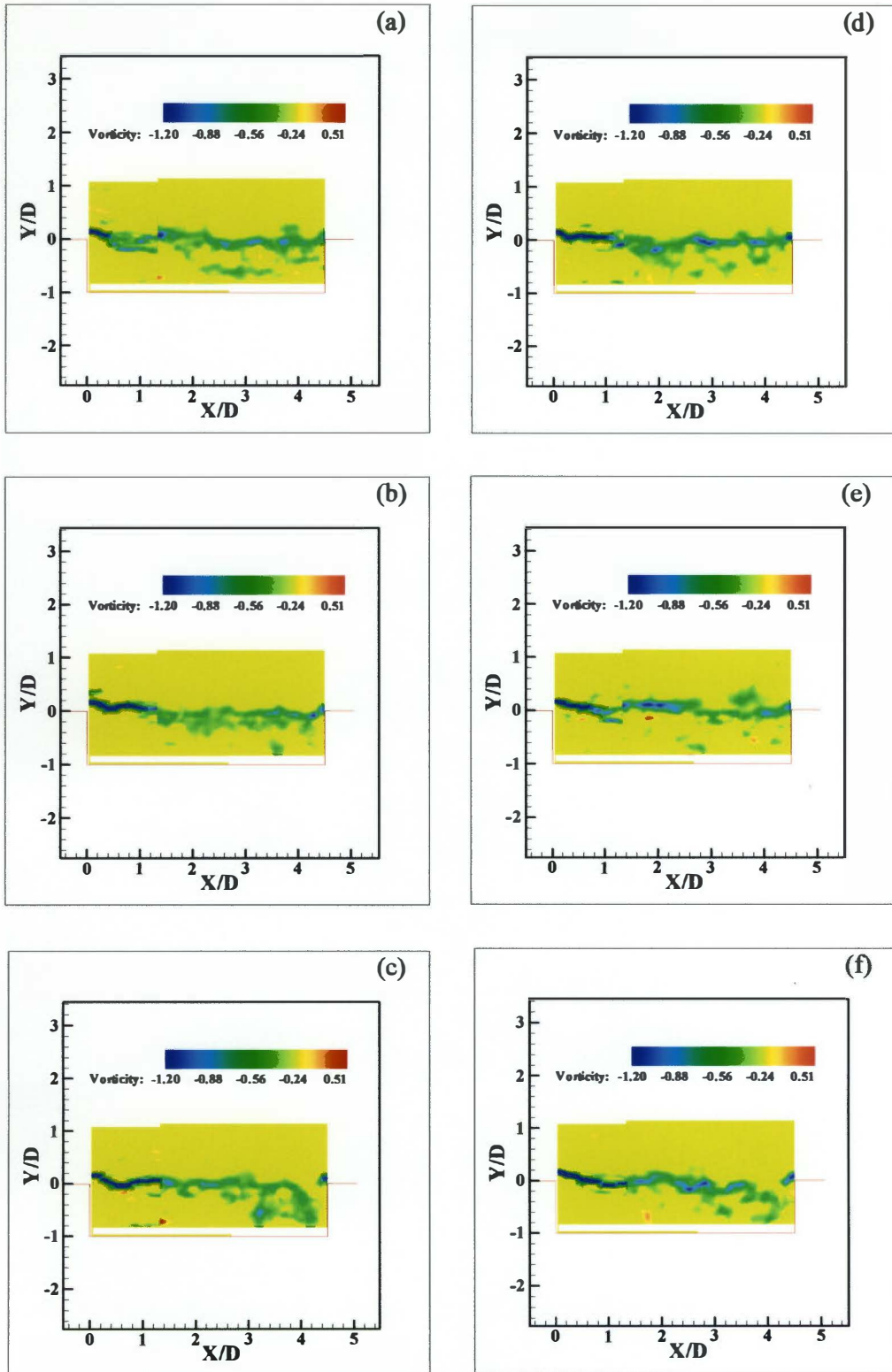


Figure 4 - 21. Instantaneous Vorticity Contours for flow over a cavity  
 $L/D = 4.5$  and freestream velocity = 214 ft/sec  
 ( 2 images taken at different times are overlapped )

## Chapter 5

### Conclusions and Future Work

An experimental study of the flow field inside selected open cavities has been conducted. Unsteady pressure and global flow field measurements were made for flow over cavities of varying dimensions ( $L/D$  ratios of 2.0, 2.67, 3.5 and 4.5 and  $W/D$  ratio of 3.33) at selected low subsonic speeds of 55 ft/sec, 160 ft/sec and 214 ft/sec.

Unsteady pressure measurements showed that flow in the cavities oscillate in the selected speed range having peak sound pressure levels of 115 to 133 dB. Two dimensional Particle Image Velocimetry gave non-intrusive instantaneous flow field measurements over and inside the selected cavities.

Velocity profiles along the length of the cavity showed the shear layer growth downstream and a re-circulation region inside the cavity. Streamtraces qualitatively gave information on the mean location of the vortex inside the cavity. The vortex depicted by the streamtraces is not steady. As  $L/D$  increased, the mean re-circulation zone was stronger and was located at the rear of the cavity.

Individual images as well as animations of the vorticity contour images clearly showed vortical disturbances in the shear layer that were convected downstream. It also showed the shear layer oscillating near the trailing edge indicating that the mass addition and removal model proposed by Heller and Bliss [6] might be applicable in these conditions.

The accuracy of the velocity profiles could have been improved if phase locked images could be taken and if ensemble averages were analysed. The pressure oscillation signals for these low speed flows were neither stationary nor sharp enough to be used uniformly as a trigger signal for phase locked measurements. Interpretation of data near the walls has an added uncertainty because of the glare. Reduction of glare from the surfaces and improved seeding would be necessary for increased accuracy of the data. Corrections for the optical distortions caused by the thickness of the optical cavity wall could also result in improved accuracy in PIV measurements along the edge of the window.

Notwithstanding these difficulties, PIV was able to provide instantaneous velocity data inside the cavity with good accuracy. With further work, the accuracy can be improved and possibly extended to locate noise sources.



**LIST OF REFERENCES**

## List of References

- [1] Rockwell, D., "Oscillation of Impinging Shear Layers", AIAA Journal, Vol. 21, No.5, May 1983, pp. 645-664
- [2] Wilcox, F.J.Jr, "Passive Venting System for Modifying Cavity Flow Fields at Supersonic Speeds", AIAA Journal, Vol. 26, No. 3, March 1998, pp. 374-376
- [3] Sarohia, V., and Massier, P.F., "Control of Cavity Noise", AIAA Journal of Aircraft, Vol. 14, No. 9, September 1977, pp. 833-837
- [4] Franke, M.E., and Carr, D.L., "Effect of Geometry on Open Cavity Flow Induced Pressure Oscillations", AIAA Paper No. 75-492, March 1975
- [5] Rossiter, J.E., "Wind Tunnel Experiments on the Flow Over Rectangular Cavities at Subsonic and Transonic Speeds", ARC R&M No. 3438, October 1964
- [6] Heller, H.H., and Bliss, D.B., "The Physical Mechanism of Flow Induced Pressure Fluctuations in Cavities and Concepts for their Suppression", AIAA Paper No. 75-491, March 1975
- [7] Vakili, A.D., Wu, J.M., and Taylor, M., "Shear Flow Control Applied to Suppress Cavity Oscillations and Improve Store Separation", Weapons Carriage and Separation Workshop, Wright Patterson AFB, Dayton, OH, April 1988
- [8] Vakili, A.D., and Gauthier, C., "Control of Cavity Flow by upstream Mass Injection", AIAA Journal of Aircraft, Vol.31, No.4, January-February 1994, pp. 169-174
- [9] Robert C. Wolfe, "An Investigation of the Effects of Upstream Mass Injection on Cavity Oscillations", Master's Thesis, University of Tennessee, Knoxville, May 1995
- [10] Chen, C.H., "Study of Subsonic and Transonic Flow Separation – With and Without Upstream Influence", Doctoral Dissertation, University of Tennessee, Knoxville, 1975
- [11] Blair, A.B.Jr, and Stallings, R.L., "Supersonic Axial Flow Characteristics of a Rectangular-Box Cavity with various Length-to-Depth ratios in a Flat Plate", NASA TM-87659, April 1986
- [12] Maureen B. Tracy and E. B. Plentovich, "Cavity Unsteady-Pressure Measurements at Subsonic and Transonic Speeds", NASA TP-3669, December 1997
- [13] Micahel J. Lucas., "Handbook of the Acoustic Characteristics of Turbomachinery Cavities", 1997
- [14] Rockwell, D., and Naudascher, E., "Review – Self Sustaining Oscillations of Flow Past Cavities", ASME Journal of Engineering, Vol. 100, No. 2, June 1978, pp. 152-165

- [15] Krishnamurthy, K., "Acoustic Radiation from Two-Dimensional Rectangular Cutouts in Aerodynamics Surfaces", NACA TN 3487, August 1955
- [16] Roshko, A., "Some Measurements of Flow in Rectangular Cutout", NACA TN 3488, August 1955
- [17] Plumblee, H.E., Gibson, J.S., and Lassiter, L.W., "A Theoretical and Experimental Investigation of the Acoustic Response of cavities in an Aerodynamic Flow", WADD-TR-16-75, March 1962
- [18] Heller, H., Holmes, D.G., and Covert, E.E., "Flow Induced Pressure Oscillations in Shallow Cavities", *Journal of Sound and Vibration*, Vol. 18, No.4, 1971, pp. 545-553
- [19] Bilanin, A.J., and Covert, E.E., "Estimation of Possible excitation Frequencies for Shallow Rectangular Cavities" *AIAA Journal*, Vol. 11, No. 3, March 1973, pp. 347-351
- [20] Heller, H., and Bliss, D., *Aerodynamically Induced Pressure Oscillations: Physical Mechanism and Suppression Concepts*, Wright-Patterson Airforce Base, Ohio, AFFDL-TR-74-133, February 1975
- [21] Sarohia, V., "Experimental Investigation of Oscillations in Flows over Shallow Cavities", *AIAA Journal*, Vol. 15, No.7, July 1977, pp. 984-991
- [22] Tam, C.K.W., and Block, P.J.W., "On the Tones and Pressure Oscillations Induced by Flow Over Rectangular Cavities", *Journal of Fluid Mechanics*, Vol. 89, Part 2, 1978, pp. 373-399
- [23] Cattafesta et al., "Experiments on Compressible Flow-Induced Cavity Oscillations", *AIAA Paper No. 98-2912*
- [24] E.F Spina, et al., "An Experimental Investigation of Flow-Induced Cavity Oscillations", *AIAA Paper No. 3705*
- [25] Tim Colonius, Amit J Basu, and Clarence W. Rowley, "Numerical Investigation of the Flow Past a Cavity", *AIAA Paper No. 99-1912*
- [26] Majdalani, J., "A Novel Flow Field Solution in a Rectangular Cavity Subject to Small Amplitude Oscillations", *AIAA Paper No. 98-2693*
- [27] Jinsong Liu, "Development and Analysis of a Low Speed Particle Image Velocimetry System", Master's Thesis, University of Tennessee, Knoxville, December 1998

## VITA

Abraham Joseph Meganathan was born on October 2, 1975 in India. He attended St. Fr. Xavier's High School in Tuticorin. He completed his undergraduate studies in Mechanical Engineering at Karunya Institute of Technology, Bharathiar University. He received his Master of Science degree in Mechanical Engineering from the University of Tennessee Space Institute and is continuing with his doctoral program.